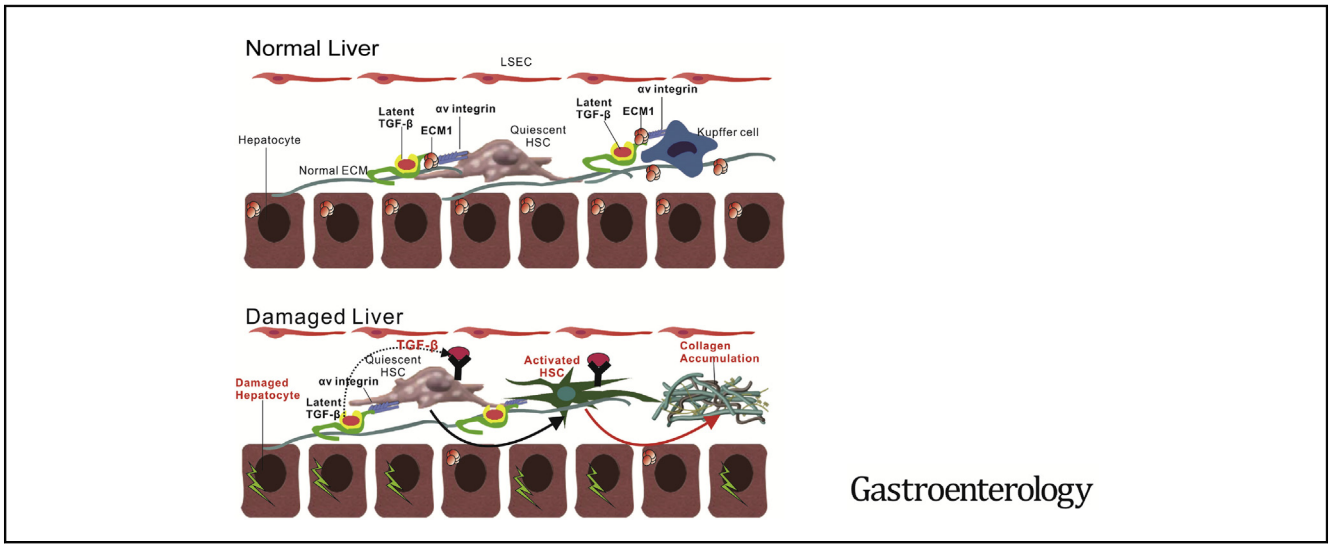
Gastroenterology 2019;157:1352–1367

ECM1 Prevents Activation of Transforming Growth Factor β, Hepatic Stellate Cells, and Fibrogenesis in Mice

Weiguo Fan,[1,2,*] **Tianhui Liu**,[3,4,*] **Wen Chen**,[2,*] Seddik Hammad,[5,6] Thomas Longerich,[7] Ingrid Hausser,[7] Yadong Fu,[8] Nan Li,[9] Yajing He,[10] Cui Liu,[1] Yaguang Zhang,[1] Qiaoshi Lian,[1] Xinhao Zhao,[1] Chenghua Yan,[1] Li Li,[2,9] Chunyan Yi,[1] Zhiyang Ling,[1] Liyan Ma,[1] Xinyan Zhao,[3,4] Hufeng Xu,[3,4] Ping Wang,[3,4] Min Cong,[3,4] Hong You,[3,4] Zhihong Liu,[10] Yan Wang,[10] Jianfeng Chen,[1] Dangsheng Li,[1] Lijian Hui,[1] Steven Dooley,[5] Jinlin Hou,[10] Jidong Jia,[3,4] and Bing Sun[1,9]

[1]State Key Laboratory of Cell Biology, CAS Center for Excellence in Molecular Cell Science, Shanghai Institute of Biochemistry and Cell Biology, Chinese Academy of Sciences; University of Chinese Academy of Sciences, Shanghai, China; [2]CAS Key Laboratory of Molecular Virology and Immunology, Institute Pasteur of Shanghai, Shanghai, Chinese Academy of Sciences, University of Chinese Academy of Sciences, Shanghai, China; [3]Liver Research Center, Beijing Friendship Hospital, Capital Medical University, Beijing, China; [4]Beijing Key Laboratory of Translational Medicine in Liver Cirrhosis and National Clinical Research Center of Digestive Disease, Beijing, China; [5]Sektion Molecular Hepatology, Department of Medicine II, Medical Faculty Mannheim, Heidelberg University, Germany; [6]Department of Forensic Medicine and Veterinary Toxicology, Faculty of Veterinary Medicine, South Valley University, Qena, Egypt; [7]Sektion Translational Gastrointestinal Pathology, Institute of Pathology, Heidelberg University, Heidelberg, Germany; [8]Institute of Shanghai Municipal Education Commission Shanghai University of Traditional Chinese Medicine, Shanghai, China; [9]School of Life Science and Technology, Shanghai Tech University, Shanghai, China; [10]Department of Infectious Diseases, Institute of Hepatology, State Key Laboratory of Organ Failure Research, Nanfang Hospital, Southern Medical University, Guangzhou, China



BACKGROUND & AIMS: Activation of TGFB (transforming growth factor β) promotes liver fibrosis by activating hepatic stellate cells (HSCs), but the mechanisms of TGFB activation are not clear. We investigated the role of ECM1 (extracellular matrix protein 1), which interacts with extracellular and structural proteins, in TGFB activation in mouse livers. **METHODS:** We performed studies with C57BL/6J mice (controls), ECM1-knockout (ECM1-KO) mice, and mice with hepatocyte-specific knockout of EMC1 ($ECM1^{\Delta hep}$). ECM1 or soluble TGFBR2 (TGFB receptor 2) were expressed in livers of mice after injection of an adeno-associated virus vector. Liver fibrosis was induced by carbon tetrachloride (CCl_4) administration. Livers were collected from mice and analyzed by histology, immunohistochemistry, in situ hybridization, and immunofluorescence analyses. Hepatocytes and HSCs were isolated from livers of mice and incubated with ECM1; production of cytokines and activation of reporter genes were quantified. Liver tissues from patients with viral or alcohol-induced hepatitis (with different stages of fibrosis) and individuals with healthy livers were analyzed by immunohistochemistry and in situ hybridization. **RESULTS:** ECM1-KO mice spontaneously developed liver fibrosis and died by 2 months of age without significant hepatocyte damage or inflammation. In liver tissues of mice, we found that ECM1 stabilized extracellular matrix–deposited TGFB in its inactive form by interacting with αv integrins

to prevent activation of HSCs. In liver tissues from patients and in mice with CCl_4-induced liver fibrosis, we found an inverse correlation between level of ECM1 and severity of fibrosis. CCl_4-induced liver fibrosis was accelerated in $ECM1^{\Delta hep}$ mice compared with control mice. Hepatocytes produced the highest levels of ECM1 in livers of mice. Ectopic expression of ECM1 or soluble TGFBR2 in liver prevented fibrogenesis in ECM1-KO mice and prolonged their survival. Ectopic expression of ECM1 in liver also reduced the severity of CCl_4-induced fibrosis in mice. **CONCLUSIONS:** ECM1, produced by hepatocytes, inhibits activation of TGFB and its activation of HSCs to prevent fibrogenesis in mouse liver. Strategies to increase levels of ECM1 in liver might be developed for treatment of fibrosis.

Keywords: Cirrhosis; Mouse Model; ECM; Integrin Signaling.

WHAT YOU NEED TO KNOW

BACKGROUND AND CONTEXT

Activation of transforming growth factor beta (TGFB) promotes liver fibrosis by activating hepatic stellate cells (HSCs). We investigated the role of extracellular matrix protein 1 (ECM1) in activation of TGFB and HSCs in livers of mice.

NEW FINDINGS

We found an inverse correlation between levels of ECM1 and severity of fibrosis severity in patients with cirrhosis, and following injection of a chemical that induces liver fibrosis in mice. ECM1 kept TGFB in its inactive form by interacting with αv integrins to prevent HSC activation and liver fibrosis.

LIMITATIONS

These studies were performed in mice and patient tissues, and we do not know the effects of ECM1 expression by different liver cell types.

IMPACT

Strategies to increase levels of ECM1 in liver might be developed for treatment of fibrosis or cirrhosis.

Hepatic fibrosis is a chronic wound-healing response to liver damage of any etiology, including chronic viral hepatitis B and C, autoimmune and biliary diseases, alcoholic steatohepatitis, and nonalcoholic steatohepatitis (NASH).[1] Fibrosis results from an imbalance in the dynamic extracellular matrix remodeling process, which leads to excessive accumulation of structural proteins in the injured liver regions, especially collagen type I. Cirrhosis is an advanced liver fibrosis stage accompanied by distortion of hepatic structure and function.[2] However, no approved treatments specifically target the mechanisms underlying fibrosis because of the potential risk of multiple adverse effects of successful experimental approaches in humans, such as interference with normal wound healing and homeostasis in other organs.[3,4]

The processes of liver injury, wound healing response, fibrogenesis, inflammation, and disease progression to cirrhosis strongly depend on dynamic cell-cell communication among hepatic cell types, primarily hepatocytes, hepatic stellate cells (HSCs), liver sinusoidal endothelial cells (LSECs), Kupffer cells (KCs), liver-resident macrophages, and diverse recruited inflammatory cell types.[5] These cells produce contextual and disease stage–related messengers and receptors that translate information into cellular pathophysiology and fate. Hepatic sinusoids are well-organized structures in the liver that facilitate contacts between cells and maintain cell function. The extracellular matrix is an important structural component of this microenvironment that stores messengers in inactive forms for immediate use in liver damage and repair.[6]

HSCs are activated in response to injury and differentiate into ACTA2-expressing, proliferating, and migrating myofibroblast-like cells that synthesize extracellular matrix proteins as a wound-closing action.[7] Activated HSCs are the primary collagen-producing cells in the liver. Transforming growth factor β, TGFB, is a cytokine that promotes fibrosis and regulates conversion of quiescent HSCs into activated HSCs.[8] TGFB is secreted as an immature, inactive complex with latent TGFB-binding proteins and GARP (glycoprotein-A repetitions predominant protein).[9,10] Latent TGFB complexes, generally present at high concentrations, are directly crosslinked to and thus deposited within the extracellular matrix.[11] Members of the integrin family that interact with a linear arginine-glycine-aspartic acid (RGD) motif can activate latent TGFB1 (and TGFB3).[12,13] In mice, disruption of genes encoding integrin components or blocking αv integrins with small molecules prevents TGFB signaling and protects against hepatic fibrosis, whereas disruption of genes encoding αv-associated integrins β3, β5, β6, or β8 does not reduce the severity of carbon tetrachloride (CCl_4)-induced liver fibrosis. These observations indicate that αv integrin–mediated activation of TGFB is required for liver fibrogenesis.[14,15] Extracellular activation of the latent complex indicates that the supply of TGFB in tissues is localized and selected to induce a fast response.[10] Little is known about the mechanisms that regulate activation of local TGFB in the liver.

Extracellular matrix protein 1, ECM1, was initially identified as an 85-kDa glycoprotein secreted by mouse osteogenic stromal cells.[16] This protein was identified amid

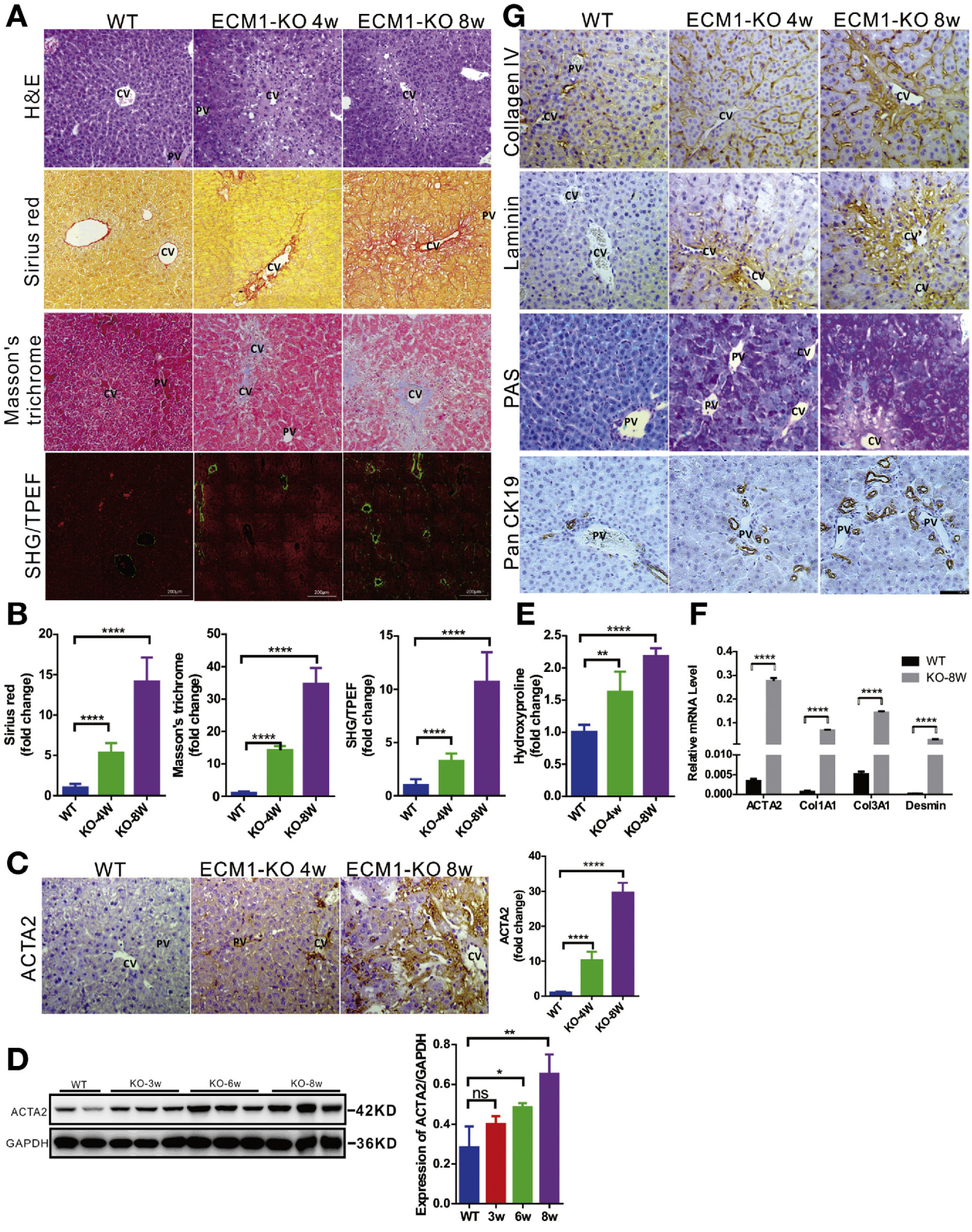
* Authors share co-first authorship.

Abbreviations used in this paper: **AAV, adeno-associated virus; CLD, chronic liver disease; CCl_4, carbon tetrachloride; ECM1, extracellular matrix protein 1; $ECM1^{\Delta;hep}$, hepatocyte-specific deletion of extracellular matrix protein 1; GAPDH, glyceraldehyde 3-phosphate dehydrogenase; GS, glutamate synthase; HSCs, hepatic stellate cells; IHC, immunohistochemistry; IL, interleukin; KC, Kupffer cell; KO, knockout; LSEC, liver sinusoidal endothelial cell; mRNA, messenger RNA; NASH, nonalcoholic steatohepatitis; SHG/TPEF, second-harmonic generation/2-photon excitation fluorescence; TGFB, transforming growth factor βl; Th, T helper; WT, wild type.**

Most current article

© 2019 by the AGA Institute. Published by Elsevier Inc. This is an open access article under the CC BY-NC-ND license (http://creativecommons.org/licenses/by-nc-nd/4.0/).

0016-5085
https://doi.org/10.1053/j.gastro.2019.07.036


A
WT
ECM1-KO 4w
ECM1-KO 8w
H&E
Sirius red
Masson's trichrome
SHG/TPEF
CV
PV
G
Collagen IV
Laminin
PAS
Pan CK19
B
Sirius red (fold change)
Masson's trichrome (fold change)
SHG/TPEF (fold change)
WT
KO-4W
KO-8W
****
E
Hydroxyproline (fold change)
**
F
Relative mRNA Level
ACTA2
Col1A1
Col3A1
Desmin
C
ACTA2
ACTA2 (fold change)
D
KO-3w
KO-6w
KO-8w
GAPDH
-42KD
-36KD
Expression of ACTA2/GAPDH
ns
*
3w
6w
8w

various extracellular matrix proteins, such as collagens, osteonectin, and bone sialoprotein.[17] ECM1 is expressed in bone and cartilage tissue,[18,19] and ECM1 gene mutations have been observed in patients with lipoid proteinosis.[20] We also reported that ECM1 affects T-helper (Th) type 2 cell migration and Th17 and Follicular helper T (T_{FH}) cell differentiation via interactions with CD122 and αv integrins.[21–23] However, little is known about the physiologic and pathologic functions of ECM1.

The present study showed that endogenous ECM1 maintains homeostasis in the architectural and functional aspects of healthy livers. Depletion of ECM1 in mice severely disturbed their liver architecture, promoted rapid liver fibrosis formation, and caused death within 2 months without inducing significant initial hepatocyte damage or inflammation. Down-regulation of ECM1 strongly increased TGFB signaling in liver cells by spontaneously activating its extracellular matrix–deposited latent form. ECM1 was predominantly produced in hepatocytes and was consistently down-regulated upon liver damage during fibrogenesis. Conditional knockout (KO) of ECM1 from hepatocytes promoted CCl_4-induced liver fibrosis. Furthermore, ECM1 expression was decreased in diseased liver from patients, and there was an inverse correlation with severity of liver fibrosis. Re-expression of ECM1 in hepatocytes of mice using an adeno-associated virus (AAV) 8 vector reduced the progression of liver fibrosis. Our combined results show that ECM1 is down-regulated in hepatocytes after liver damage, which activates TGFB1 in the matrix to facilitate HSC activation and fibrogenesis. Strategies to re-express ECM1 in hepatocytes might be developed for treatment of liver fibrosis.

Materials and Methods

Human Samples

Human liver fibrosis samples were provided by the tissue bank in accordance with its regulations and with approval of the ethics committee of Heidelberg University, Beijing Friendship Hospital, and Nanfang Hospital. The investigated data set of patients with alcoholic hepatitis is deposited at the National Center for Biotechnology Information (accession number GSE28619).

Animals

All mice were of the C57BL/6J background. ECM1-KO mice have been described previously.[22] All ECM1 wild type (WT) and ECM1-KO mice were generated from ECM1 heterozygous mice. Albumin-Cre mice were purchased from Shanghai Biomodel Organism (Shanghai, China). $ECM1^{fl/fl}$ mice with a loxP-flanked ECM1 allele on a C57BL/6J background were generated by Shanghai Biomodel Organism (see the Supplementary Materials and Methods for details). Albumin-Cre mice were crossed with $ECM1^{fl/fl}$ mice to produce $ECM1^{fl/fl}$/Alb-Cre mice. All experiments were conducted with male mice. ABCB4-KO mice represent a cholestasis-driven chronic liver disease (CLD) according to Smit et al[24] and multiple additional studies. The presented analysis is representative for 44-week-old male ABCB4-KO mice (BALBc background) according to Hammad et al.[25] Mice were housed in laboratory cages at 23 ± 3°C at 35% ± 5% humidity under a 12-hour dark/light cycle. With free access to a regular chow diet (Shanghai Laboratory Animal Company, Shanghai, China), all mice were maintained under specific pathogen-free conditions. All protocols of animal experiments were approved by the Institutional Animal Care and Use Committee at the Institute Pasteur of Shanghai, Shanghai Institutes for Biological Sciences, Chinese Academy of Sciences (Shanghai, China).

Statistical Analysis

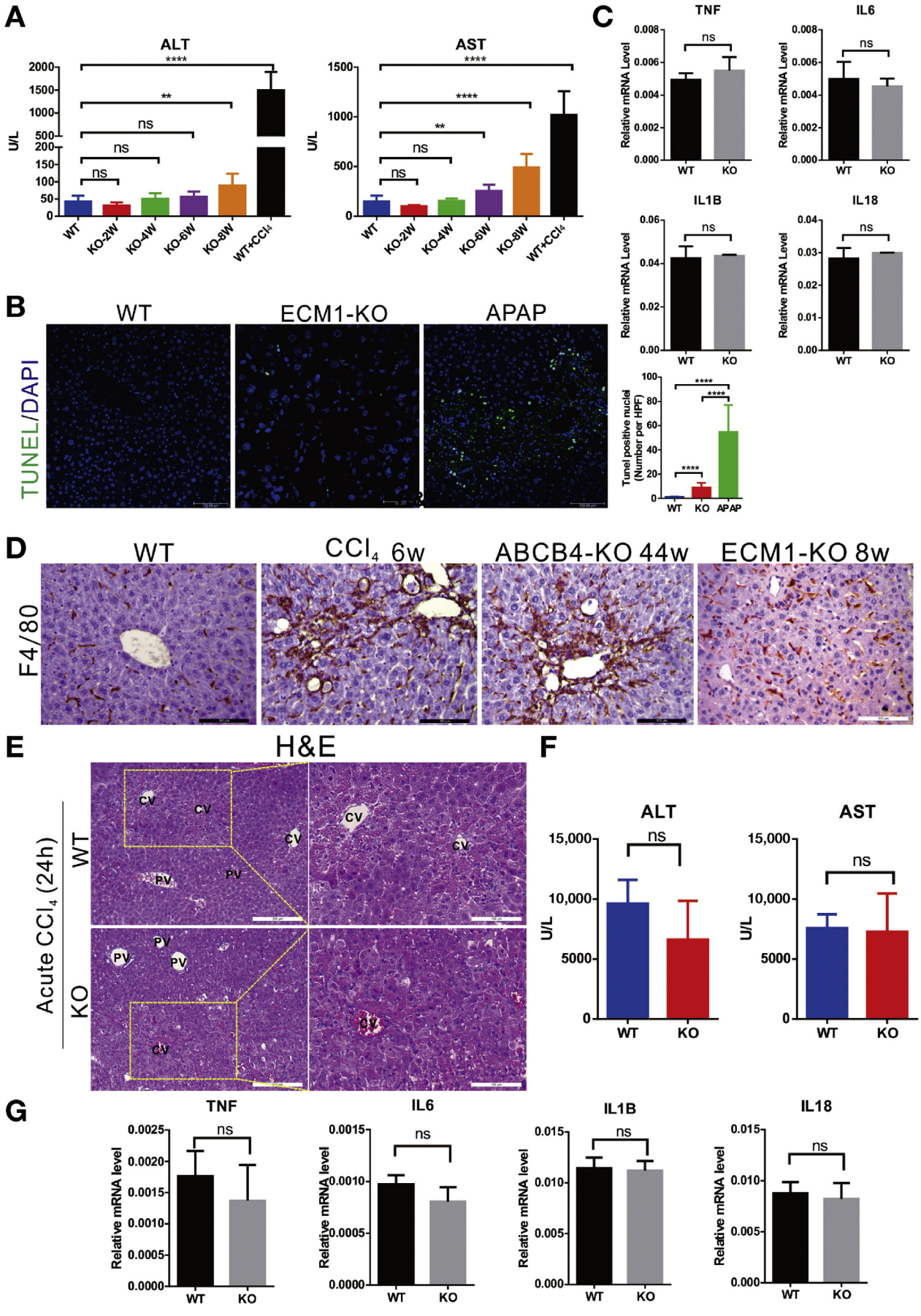
Comparisons between 2 different groups were performed with the unpaired 2-tailed Student t test. Values of $P < .05$ were considered statistically significant. Statistical analyses were performed using Prism 5 software (GraphPad, San Diego, CA).

Results

Genetic Abrogation of ECM1 Induces Spontaneous Liver Fibrosis With Distinguished Morphologic and Histopathologic Features

Among several organs assessed in healthy mice, the liver had the highest expression of ECM1 at the RNA and protein levels. Fluorescence microscopy showed that ECM1 is predominantly localized in the perisinusoidal space (Supplementary Figure 1), suggesting that ECM1 is an extracellular matrix component in the hepatic

Figure 1. ECM1-KO mice spontaneously develop symptoms of severe liver fibrosis 8 weeks after birth. (*A*) Representative histologic images. Liver sections from ECM1-WT and ECM1-KO mice were stained with H&E, Sirius Red, and Masson's trichrome and scanned with SHG/TPEF microscopy. ECM1-KO mice display a disrupted liver architecture and increased collagen deposition. (*B*) Sirius Red staining is quantified by ImageJ (National Institutes of Health, Bethesda, MD) analysis, counted in 10 different fields for each sample, 2 samples from each mouse, and presented as fold change compared with the control; n = 8. Only male mice were used. (*C*) Representative images and quantification of ACTA2 via IHC analyses of sections from the livers of ECM1-WT and ECM1-KO mice as shown in (*B*). (*D*) Representative immunoblot and quantification of ACTA2 protein expression. Glyceraldehyde 3-phosphate dehydrogenase (GAPDH) was used as a loading control. (*E*) Hydroxyproline levels in the livers of 8-week-old male mice. Data represent the fold change compared with WT mice, which was set to 1; n = 8 male mice/group. (*F*) Relative mRNA levels of ACTA2, Col1A1, Col1a3, and desmin in nonparenchymal cells purified from WT/KO male mice at 8 weeks of age, quantified using quantitative reverse-transcription polymerase chain reaction. Results were normalized to GAPDH; n = 4 male mice/genotype. (*G*) Representative histologic and IHC staining images. Sections from the livers of ECM1-WT and ECM1-KO mice were probed with antibodies for collagen IV, laminin, and Pan CK19 (ductular reaction) and stained with periodic acid–Schiff. The results are shown as the mean ± standard deviation. $^{**}P < .01$, $^{****}P < .0001$ (Student t test). Scale bar, 100 μm and 200 μm (SHG/TPEF). SMA, smooth muscle actin; w, week.


A
ALT
AST
U/L
WT
KO-2W
KO-4W
KO-6W
KO-8W
WT+CCl4
ns
**
****
B
WT
ECM1-KO
APAP
TUNEL/DAPI
C
TNF
IL6
IL1B
IL18
Relative mRNA Level
Tunel positive nuclei (Number per HPF)
D
WT
CCl4 6w
ABCB4-KO 44w
ECM1-KO 8w
F4/80
E
H&E
Acute CCl4 (24h)
CV
PV
F
ALT
AST
G
TNF
IL6
IL1B
IL18
Relative mRNA level

sinusoids of a normal liver. ECM1-KO mice showed macroscopic manifestation of severe fibrosis, such as weight loss and ascites, at approximately 8 weeks of age. Livers from ECM1-KO mice had a rough surface and increased stiffness (Supplementary Figure 2). ECM1-KO mice generally did not survive past the age of 6 to 8 weeks. Liver sections were stained with H&E, Sirius Red, and Masson's trichrome and examined with second-harmonic generation/2-photon excitation fluorescence (SHG/TPEF) microscopy. Histologic analyses showed that ECM1-KO mice had time-dependent progressive perisinusoidal fibrosis, as shown by massive extracellular matrix deposition at the age of 8 weeks (Figure 1*A* and *B*), compared with WT mice maintained under the same conditions. Furthermore, the disease was significantly more severe than other typical liver fibrosis mouse models (eg, chronic CCl_4-treated and ABCB4-KO mice) (Supplementary Figure 3). In parallel, the number of ACTA2-positive cells was dramatically increased in the sinusoidal spaces (Figure 1*C* and *D*), indicating that the observed extracellular matrix was predominantly synthesized by activated HSCs. Quantification of the hepatic hydroxyproline content and examination of the messenger RNA (mRNA) expression of key fibrotic marker genes (eg, ACTA2, desmin, Col1A1, and Col3A1), further support the occurrence of spontaneous liver fibrogenesis in ECM1-KO mice ($P < .05$, by t test) (Figure 1*E* and *F*).

To more thoroughly delineate the type of liver damage and fibrosis in ECM1-KO mice, we performed several additional analyses. Based on the skin phenotype in ECM1-mutated patients with lipoid proteinosis,[20] we assessed whether ECM1 deletion could disturb basement membrane protein expression and localization in the mouse liver. Indeed, methylene blue staining of resin-embedded material showed a pronounced thickening of the venular basement membranes and respective perivenular sinusoids in the ECM1-KO mice (Supplementary Figure 4*A*). In ultrastructural analysis, excessive, mostly amorphous, irregularly deposited material was visible that extended into the perivenular sinusoids, which normally lack a continuous basement membrane (Supplementary Figure 4*B*). This phenomenon was confirmed by immunohistochemistry (IHC), which showed increased perisinusoidal collagen IV and laminin expression in the perivenular area of the liver acini (Figure 1*G*). The ECM1-KO mice therefore had age-dependent progression of basement-like material deposition, collapsed perivenular parenchyma, bridged necrosis development with condensation of the reticulin network, and formation of perisinusoidal septa after 8 weeks. This was further shown by periodic acid–Schiff and Gomori staining (Figure 1*G* and Supplementary Figure 5).

To gain further insight into the adverse effects of ECM1 depletion on liver architecture and function, we investigated the biliary and sinusoidal vessel system and liver zonation by immunofluorescence staining (Supplementary Figures 6 and 7). In ECM1-KO mice, the first layer of glutamine synthetase (GS)-positive hepatocytes was lost, indicating a significant effect on liver zonation. However, this effect was not due to apoptosis of the GS-positive cells themselves (Supplementary Figure 6*B*). Next, microvessels and bile networks were visualized by PECAM and DPPIV/CD26 staining. Both networks were dramatically altered as the microvessel density was decreased and the vessels were dilated (Supplementary Figure 7*A*). The bile canaliculi appeared curly, irregular, and dilated (Supplementary Figure 7*B*). Finally, a significant ductular reaction, which represents proliferative bile duct epithelial cells, was obvious in ECM1-KO mice, as visualized by PanCK and CK19 staining (Figure 1*G* and Supplementary Figure 7*C* and *D*). Thus, partial loss of GS-positive hepatocytes, ductular reaction, microvessel disorganization, and bile networks are associated with ECM1 depletion in the liver. These data suggest that ECM1 is critical for the maintenance of normal architecture and physiologic homeostasis of cell-cell communication in the healthy liver. In conclusion, depletion of ECM1 expression is sufficient to spontaneously activate HSCs, initiate fibrogenesis, and induce severe fibrosis-like disturbance of the liver architecture, ultimately leading to death.

ECM1 Inhibits Hepatic Stellate Cell Activation Via Blocking TGFB Activation Rather Than Affecting Hepatocyte Death and Inflammation

Liver damage-induced inflammation and HSC activation are typical features of progressive fibrogenesis. Most

Figure 2. ECM1-KO mouse livers show weak liver damage and inflammation during fibrogenesis. (*A*) Aspartate aminotransferase (AST) and alanine aminotransferase (ALT) levels in the sera of ECM1-KO mice compared with those in the sera of WT and mice chronically treated with CCl_4 for 6 weeks (n = 8 male mice/group). (*B*) TUNEL staining of apoptotic cells in liver sections (n = 10 male mice/group). (*C*) The relative mRNA levels of tumor necrosis factor α, IL-6, IL-1, and IL-18 in nonparenchymal cells isolated from WT/KO mice at 8 weeks of age were quantified using quantitative reverse-transcription polymerase chain reaction, and the results were normalized to GAPDH (n = 4 male mice/genotype). The results are shown as the mean ± standard deviation. (*D*) F4/80 staining of KCs/macrophages in liver sections of 8-week-old ECM1-WT and ECM1-KO mice compared with those in diseased livers from mice chronically treated with CCl_4 for 6 weeks and 44-week-old ABCB4-KO mice. (*E*) Representative H&E images of livers 24 hours after a single administration of 1.6 g/kg CCl_4. Scale bars, 200 μm and 100 μm for overviews and close-up images, respectively. (*F*) Levels of the liver enzymes ALT and AST in circulating blood from mice exposed for 24 hours to confirm tissue damage (n = 8 male mice/genotype). (*G*) The relative mRNA levels of inflammatory cytokines 24 hours after CCl_4 injection in ECM1-KO mice and WT controls were quantified using qRT-PCR and normalized to GAPDH (n = 8 male mice/genotype). The results are shown as the mean ± standard deviation. Student t test: $^{**}P < .01$, $^{****}P < .0001$. ns, nonsignificant difference.

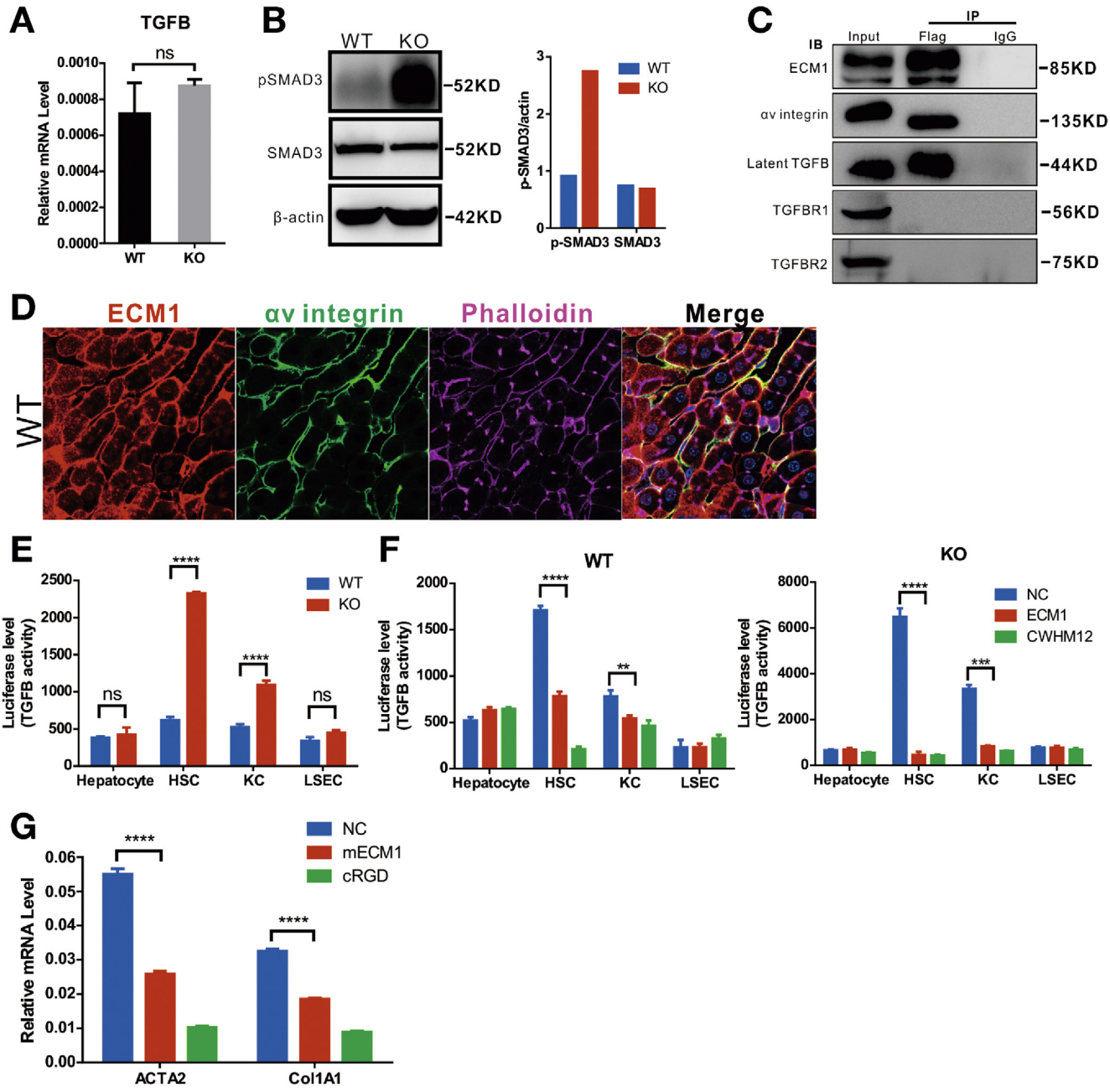


Figure 3. ECM1 deficiency leads to spontaneous activation of extracellular matrix–stored latent TGFB and accelerated myofibroblast generation. (*A*, *B*) Nonparenchymal cells were purified from 8-week-old ECM1-WT and KO mouse livers. (*A*) Relative mRNA levels of TGFB. (*B*) Representative immunoblot and quantification of phosphorylated SMAD3/SMAD3 protein levels. β-actin was used as a loading control (n = 4 male mice/genotype). (*C*) Immunoprecipitation studies: ECM1-KO mice infected with AAV-ECM1 for re-expression of 3 × Flag-tagged ECM1 protein in liver. An anti-flag antibody was used for immunoprecipitation (IP), and then ECM1, αv integrin, latent TGFB, and TGFB receptor antibodies were used for immunoblotting (IB). (*D*) Immunofluorescent staining of liver sections from WT mice using ECM1 and αv integrin antibodies; phalloidin was used to display cell membranes. (*E*, *F*) TGFB activation studies, using the coculture of primary liver cells from ECM1-WT and KO mice with NIH3T3-TGFB signaling reporter cells. Reporter cells were cultured without fetal bovine serum for 48 hours before coculture to avoid the effects of TGFB in serum. (*E*) TGFB activity was examined after coculture for 24 hours. (*F*) Cells were cocultured with or without recombinant mouse ECM1 (50 μg/mL) and CWHM12 (10 μg/mL), as indicated. In this setting, HSCs were cultured for 5 days before being cocultured with TGFB signaling reporter cells (n = 4 male mice/group). (*G*) Relative mRNA levels of ACTA2 and Col1A1 in primary mouse HSCs, as determined by quantitative reverse-transcription polymerase chain reaction. HSCs were isolated from WT mice and activated in culture for 14 days with or without recombinant ECM1 and cyclic arginine-glycine-aspartic acid (10 μg/mL), as indicated (n = 4 male mice/group).

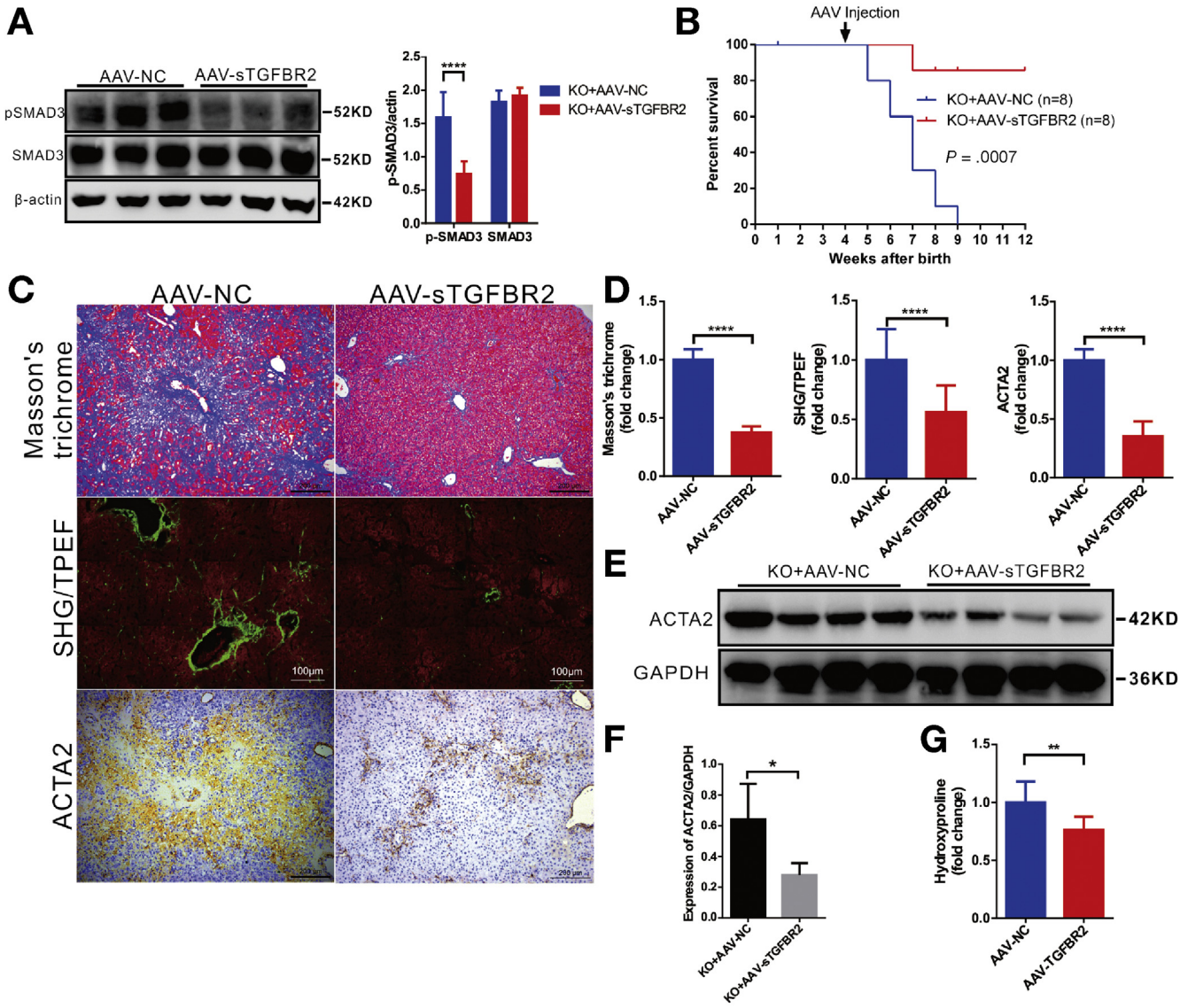
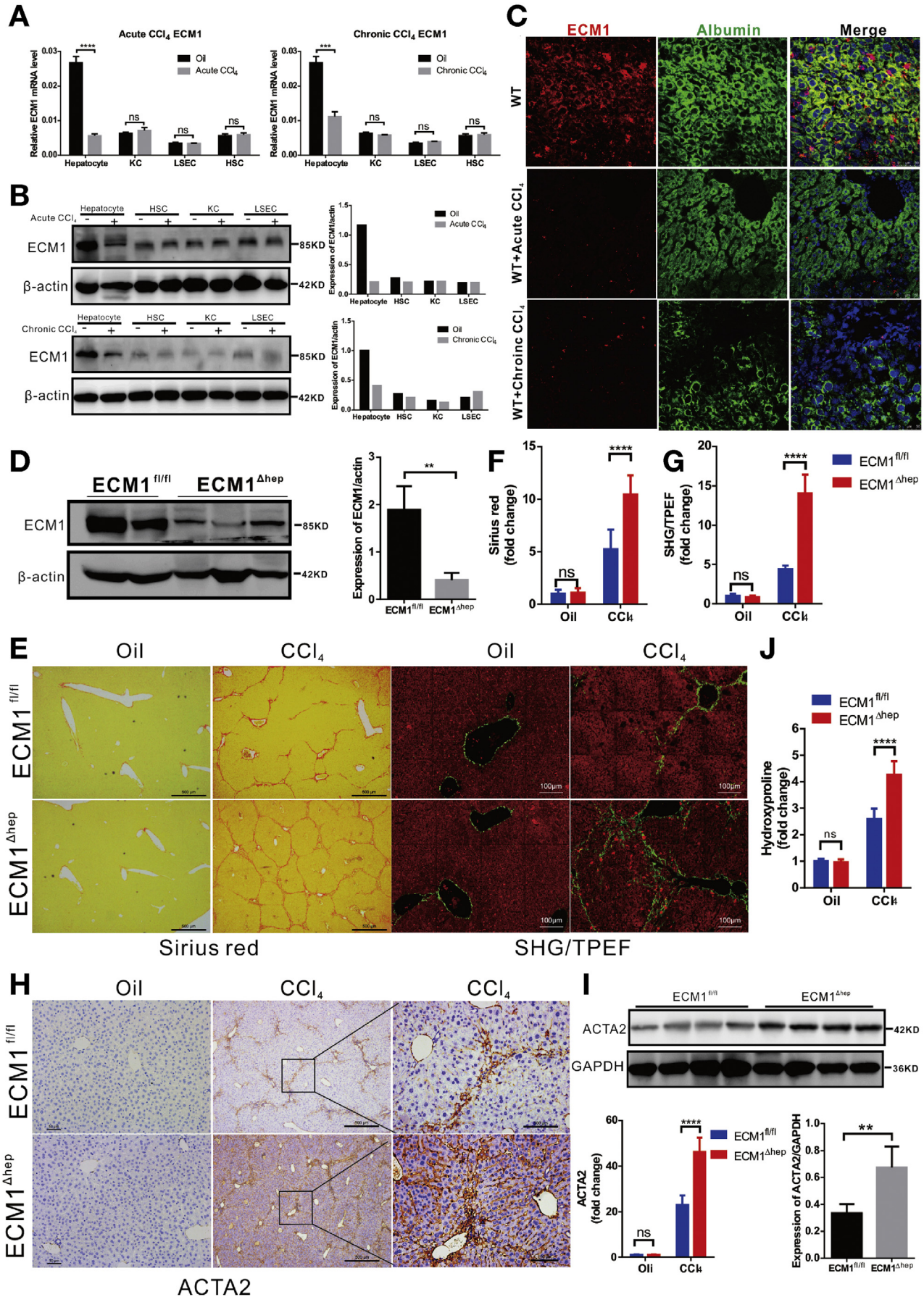


Figure 4. Blunting TGFB activity rescues ECM1-KO mice from spontaneous fibrosis. ECM1-KO mice were injected with AAV-NC or AAV-sTGFBR2 at the age of 4 weeks. (*A*) Representative immunoblot and quantification showing the expression and phosphorylation of SMAD3 in liver lysates. β-Actin was used as a loading control (n = 3 male mice/group). (*B*) Survival curves of mice infected with AAV-NC or AAV-sTGFBR2 (n = 8 male mice/group). (*C*) Histologic and immunohistochemical analyses of liver sections. Scale bar, 100 μm (SHG/TPEF) and 200 μm (Masson's trichrome and ACTA). (*D*) Quantification of Masson's trichrome staining, SHG/TPEF scanning, and ACTA2 IHC staining. (*E*, *F*) Representative immunoblot and quantification of ACTA2 protein expression. GAPDH was used as a loading control (n = 4 male mice/group). (*G*) Hydroxyproline levels in the livers of mice infected with AAV-NC or AAV-sTGFBR2 (n = 8 male mice/group). The results are shown as the mean ± standard deviation. Student *t* test: $^{*}P < .05$, $^{**}P < .01$, and $^{****}P < .0001$. ns, nonsignificant difference.

mice with liver fibrosis models have massive hepatocyte death and increased inflammation before HSC activation and collagen production. Unexpectedly, the observed hepatocyte damage and inflammation were weak in the disease progression dynamics of ECM1-KO mice, compared with those in mice given CCl_4 or ABCB4-KO mice. Briefly, the alanine aminotransferase and aspartate aminotransferase levels in the blood of ECM1-KO mice increased slightly only shortly before the mice died (Figure 2*A*). This result was in line with the lack of significant hepatocyte apoptosis in ECM-KO mice, as indicated by terminal deoxynucleotidyl transferase–mediated deoxyuridine triphosphate nick-end labeling staining, compared with that in the acetaminophen-damaged mouse liver, which served as a positive control ($P < .0001$ by *t* test) (Figure 2*B*). Regarding inflammation, ECM1-KO mice did not display elevated levels of inflammatory cytokines, such as tumor necrosis factor α, interleukin (IL) 6, IL-1B, and IL-18 ($P > .05$, by t test) (Figure 2*C*). Consistent with this result, the number of F4/80-positive tissue-infiltrating hepatic macrophages/KCs was largely unaltered in ECM1-KO mice compared with



BASIC AND TRANSLATIONAL LIVER

that in WT mice and in contrast to the fibrotic livers of chronic CCl_4-treated and ABCB4-KO mice (Figure 2*D*).

Histologic analysis of the necrotic area upon acute CCl_4 insult showed no obvious quantitative difference in liver damage between the tested genotypes (Figure 2*E*), which was also reflected by the levels of the circulating liver enzymes alanine aminotransferase and aspartate aminotransferase (Figure 2*F*). Of note, ECM1 deletion was associated with a more diffuse pattern of cell necrosis compared with WT mice, probably due to the disturbance of liver zonation in KO mice. The expression levels of typical inflammatory markers were not increased in the ECM1-KO mice at 24 hours after CCl_4 injection (Figure 2*G*). In conclusion, ECM1 is not a detrimental factor underlying acute damage and inflammation in the liver.

TGFB mRNA levels were not significantly different between ECM1-KO and WT mice ($P > .05$ by t test) (Figure 3*A*). However, TGFB signaling activation, as determined by SMAD3 phosphorylation levels, was greatly induced in the ECM1-KO mice (Figure 3*B*). Our previous work showed that ECM1 may interact with αv integrins on dendritic cells and may thus interfere with the activation of latent TGFB.[21] We next confirmed that ECM1, αv integrin, and latent TGFB interact and colocalize in the hepatic sinusoid (Figure 3*C* and *D*). To investigate whether ECM1 affects the latency of TGFB in the liver, which then translates to HSC activation, we investigated the activation of latent TGFB ex vivo. We isolated hepatocytes, HSCs, KCs, and LSECs from ECM1-WT and -KO mice and cocultured them with NIH-3T3 cells stably expressing a luciferase reporter vector containing 4 repeats of a SMAD-binding element upstream of the minimal promoter of the firefly luciferase coding region. As expected, HSCs were the main producers of (active) TGFB in the liver, and KCs also contributed. No effect on reporter gene activation was observed in ECM1 gene–depleted hepatocytes and LSECs compared with that in WT controls, probably because these cells were not TGFB producers in our experimental setting ($P < .0001$ by t test) (Figure 3*F*). HSCs from KO mice were activated faster and differentiated into ACTA2-expressing myofibroblast-like cells faster than those from WT mice, which was consistent with our results showing that the number of ACTA2-positive cells was increased in the sinusoidal space of ECM1-KO mice (Figure 1*C*).

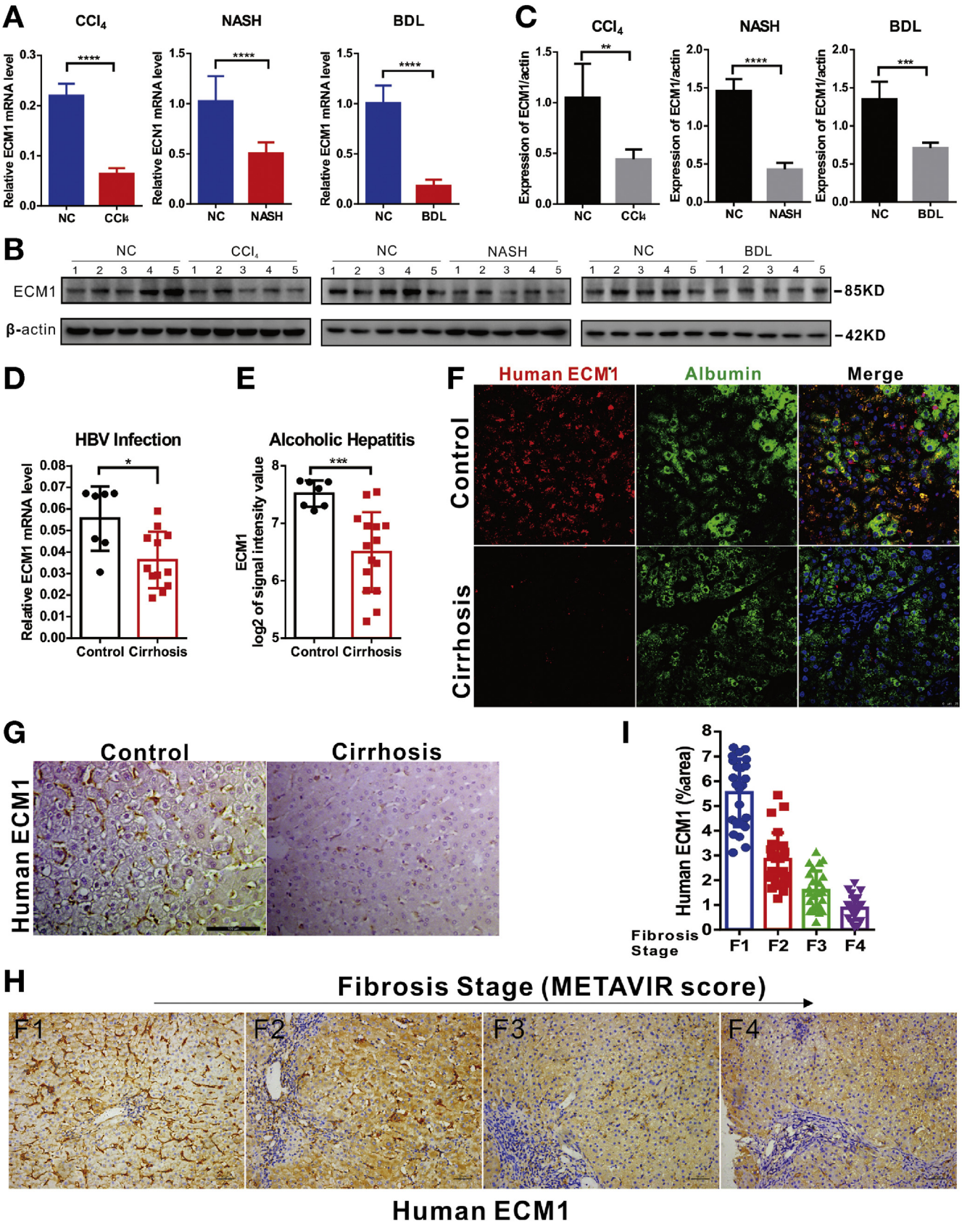
Adding recombinant mouse ECM1 protein significantly inhibited luciferase expression and HSC activation, as estimated by ACTA2 and Col1A1 gene expression levels ($P < .0001$ by t test) (Figure 3*G*). The cyclic arginine-glycine-aspartic acid and CWHM12 peptides have been shown to inhibit latent TGFB activation by disrupting the interaction of αv integrin and latent TGFB[14,26] and were included as positive controls, displaying results very similar to those achieved with the recombinant ECM1 protein. Because activated HSCs display high αv integrin and latent TGFB levels[14] and based on our own data described here and previously,[21] we suggest that ECM1 interacts with αv integrins and latent TGFB in the extracellular space to maintain latency.

To functionally prove this connection in vivo, we blunted TGFB signaling in the ECM1-KO mouse liver using AAV serotype 8 infection-mediated expression of a soluble TGFB type II receptor with a human IgG Fc tag (AAV-sTGFBR2 [soluble TGFB type II receptor]), previously shown to inhibit TGFB signaling, HSC activation, and liver fibrosis in vivo.[27–29] Upon expression in hepatocytes, the signaling-deficient soluble receptor is secreted and captures activated TGFB ligands, thereby avoiding the formation of signaling receptor complexes. Tail vein injection of the construct into 4-week-old ECM1-KO mice decreased SMAD3 phosphorylation levels in most animals compared with those in green fluorescent protein–expressing controls (AAV-NC) (Figure 4*A*). Ectopic expression of sTGFBR2 rescued the ECM1-KO liver phenotype ($P < .001$ by t test) (Figure 4*B*). Most sTGFBR2-expressing mice survived, and macroscopic, histologic, and biochemical examinations of their livers showed decreased collagen deposition and ACTA2-positive HSCs, as well as reduced hydroxyproline levels ($P < .01$ by t test) (Figure 4*C*–*G*). Taken together, these results suggest that the spontaneous hepatic fibrosis observed in ECM1-KO mice was, to a large extent, a consequence of locally increased latent TGFB activation in the liver.

Hepatocytes Are the Major ECM1 Producers in a Healthy Liver

The main cell types in the liver are hepatocytes and nonparenchymal cells of the space of Disse, such as LSECs, HSCs, and KCs. To identify the cell type responsible for

Figure 5. Depleting ECM1 in hepatocytes enhances CCl_4-mediated liver fibrosis. (*A*) mRNA and (*B*) protein expression of ECM1 in different liver cell types from control (olive oil–treated), acute CCl_4-treated, and chronic CCl_4-treated (2 times per week for 4 weeks) mice (n = 4 male mice/group). (*C*) ECM1 mRNA in situ hybridization on fixed frozen liver tissue using RNAscope. (*D*) Representative immunoblot and quantification of ECM1 protein in the livers of $ECM1^{fl/fl}$ and $ECM1^{\Delta hep}$ mice. β-actin was used as a loading control. (*E*) Representative images of Sirius Red–stained and SHG/TPEF-scanned liver sections from $ECM1^{fl/fl}$ and $ECM1^{\Delta hep}$ mice treated with oil or CCl_4 for 4 weeks. Scale bars, 500 μm (Sirius red) and 100 μm (SHG/TPEF). (*F*, *G*) Quantification of (*F*) Sirius Red staining and (*G*) SHG/TPEF scanning (n = 8 male mice/group). (*H*) Representative images and quantification of ACTA2 IHC analyses of liver sections from $ECM1^{fl/fl}$ and $ECM1^{\Delta hep}$ mice (n = 8 male mice/group). (*I*) Representative immunoblot and quantification of ACTA2 protein expression. GAPDH was used as a loading control (n = 4 male mice/group). (*J*) Hydroxyproline levels in the livers of $ECM1^{fl/fl}$ and $ECM1^{\Delta hep}$ mice treated with oil or CCl_4 for 4 weeks (n = 8 male mice/group). The results are shown as the mean ± standard deviation. Student t test: $^*P < .05$, $^{**}P < .01$, $^{****}P < .0001$. ns, nonsignificant difference; SMA, smooth muscle actin.


A
CCl4
NASH
BDL
Relative ECM1 mRNA level
Relative ECN1 mRNA level
NC
CCl4
NASH
BDL
C
Expression of ECM1/actin
B
ECM1
β-actin
85KD
42KD
D
HBV Infection
Relative ECM1 mRNA level
Control Cirrhosis
E
Alcoholic Hepatitis
ECM1
log2 of signal intensity value
F
Human ECM1
Albumin
Merge
Control
Cirrhosis
G
Control
Cirrhosis
Human ECM1
I
Human ECM1 (%area)
Fibrosis Stage
F1 F2 F3 F4
H
Fibrosis Stage (METAVIR score)
F1 F2 F3 F4
Human ECM1

ECM1 production, we purified the different liver cell types from a healthy liver and examined ECM1 mRNA and protein expression. Surprisingly, hepatocytes were the major, but not only, cellular source of ECM1 in the mouse liver. However, ECM1 was down-regulated in only hepatocytes upon acute and chronic liver damage ($P < .0001$ by t test) (Figure 5*A* and *B*). To confirm this finding directly in liver tissue, we used ECM1 and albumin mRNA from fixed, frozen liver tissue samples to perform in situ hybridization using the RNAscope system (ACD, Palo Alto, CA) (Figure 5*C*).

To assess the effect of hepatocyte-depleted ECM1 on the fate of the liver, we generated mice with a loxP-flanked ECM1 allele ($ECM1^{fl/fl}$) and crossed them with mice carrying a transgene encoding Cre recombinase under the control of the albumin enhancer promoter (Alb-Cre) (Supplementary Figure 8*A* and *B*). The cross-generated Alb-Cre/$ECM1^{fl/fl}$ mice (hereafter called *$ECM1^{\Delta hep}$ mice*) with a hepatocyte-specific (conditional) ECM1 deficiency (Supplementary Figure 8*C* and *D*) had significantly decreased liver ECM1 protein levels (Figure 5*D*). However, no spontaneous fibrosis phenotype was induced, which was probably due to the compensation of ECM1 synthesis by other cell types. We injected $ECM1^{\Delta hep}$ mice and their littermate controls with CCl_4 twice weekly for 4 weeks. The $ECM1^{\Delta hep}$ mice had a higher degree of liver fibrosis (Figure 5*E*–*G*) and HSC activation than control mice given CCl_4 (Figure 5*H* and *I*). Consistent with these morphologic observations, the liver hydroxyproline content was higher in $ECM1^{\Delta hep}$ mice than in control mice ($P < .0001$ by t test) (Figure 5*J*). Collectively, these results confirm that reducing ECM1 production and secretion selectively in hepatocytes facilitates hepatic fibrogenesis upon injury.

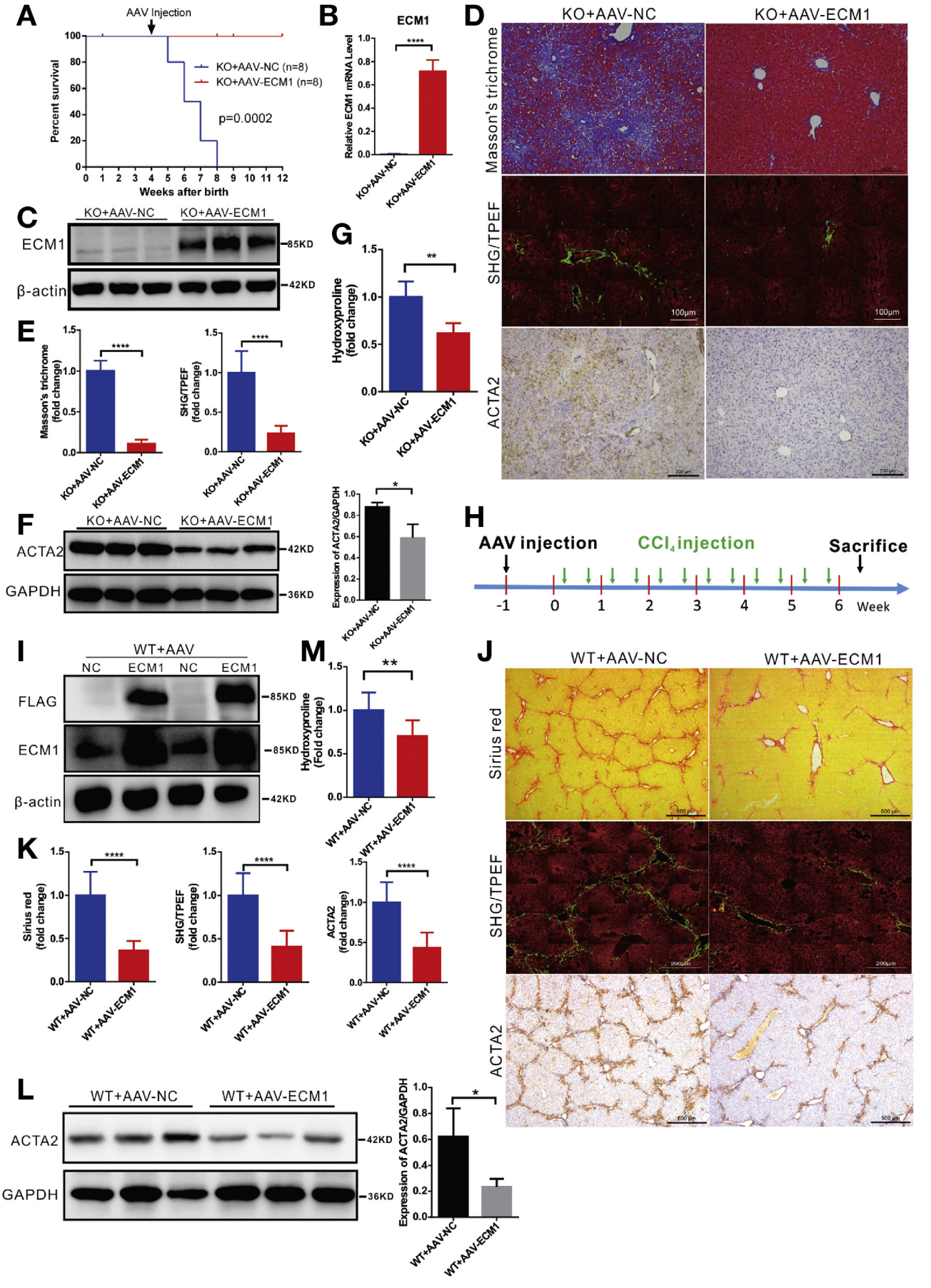
ECM1 Expression Decreases During Liver Fibrogenesis Progression

To systematically confirm that ECM1 expression is down-regulated by liver damage and fibrogenesis, we used 3 widely used mouse models of CLD: injection of CCl_4, high-fat diet to induce NASH, and surgical bile duct ligation.[30] ECM1 expression was consistently decreased in the livers of all mouse models tested during progressive fibrosis ($P < .0001$ by t test) (Figure 6*A*–*C*). To translate our findings in mice to patients with CLD, we analyzed ECM1 expression in cohorts of patients with CLDs from different causes. We found decreased ECM1 mRNA levels in cirrhotic liver samples from patients with hepatitis B virus infection and in samples from a cohort of patients with severe alcoholic hepatitis compared with those in the respective healthy control samples ($P < .05$ and $P < .001$, respectively, by t test) (Figure 6*D* and *E*). The ECM1 and albumin mRNA in situ hybridization confirmed that hepatocytes are the major source of ECM1 in the human liver and that ECM1 is down-regulated during fibrosis (Figure 6*F*). In addition to mRNA, progressive down-regulation of ECM1 protein expression in the human cirrhotic liver was also confirmed by IHC analyses (Figure 6*G*). Liver fibrosis severity is scored based on METAVIR stages F0 to F4, in which grade F4 indicates cirrhosis. In correlation studies with clinical data, the decreased ECM1 expression was associated with more severe fibrosis progression (Figure 6*H* and *I*). Collectively, these data suggest that the physiologic presence of ECM1 in the liver is required to maintain tissue homeostasis and that reduced hepatocytic ECM1 production induced by injury leads to HSC activation and, consequently, to liver fibrosis.

Ectopic ECM1 Expression in Hepatocytes Reverses Carbon Tetrachloride–Induced Hepatic Fibrogenesis

Our data suggest that ECM1 is an important local regulator of fibrosis in the liver, and its therapeutic potential is obvious. To test this and confirm the direct contribution of ECM1 to liver fibrogenesis, we performed rescue experiments by ectopically expressing ECM1 in ECM1-KO mice using an AAV serotype 8 vector. We injected AAV-ECM1 with a FLAG tag at the N terminus (AAV-ECM1) or a control AAV vector (AAV-NC) into the tail veins of ECM1-KO mice. AAV-ECM1 injection resulted in up-regulated ECM1 expression in ECM1-KO mice livers 4 weeks after injection (Figure 7*A*–*C*). ECM1-KO mice injected with the control AAV generally did not survive longer than 8 weeks, whereas all AAV-ECM1–injected ECM1-KO mice survived and had no symptoms of severe fibrosis ($P < .001$ by t test) (Figure 7*A*). Histologic analyses showed that treatment with AAV-ECM1 significantly

Figure 6. ECM1 expression decreases during liver fibrosis progression. (*A*–*C*) Mice were challenged with CCl_4 (2 times per week for 4 weeks); fed a high-fat, methionine- and choline-deficient diet (8 weeks); or underwent bile duct ligation (9 days). (*A*) The mRNA expression of ECM1 was assessed in the mouse livers (n = 8 male mice/group). (*B*) Representative immunoblot and (*C*) quantification of ECM1 protein expression. β-actin was used as a reference (n = 5 male mice/group). (*D*, *E*) Relative mRNA levels of ECM1 in liver biopsy samples from healthy control individuals and cohorts of patients with (*D*) hepatitis B virus infection or (*E*) alcoholic hepatitis as quantified by quantitative reverse-transcription polymerase chain reaction or estimated from microarray data. (*F*) Human ECM1 mRNA in situ hybridization on healthy control and cirrhosis liver tissue using the RNAscope. (*G*) Representative IHC analysis of ECM1 in liver sections from a representative healthy control individual and patient with hepatitis B virus infection. (*H*) ECM1 expression in liver biopsy samples from a cohort of patients with hepatitis B virus presenting with various stages of fibrosis (n = 20 patients in each F stage) as determined by IHC. (*I*) Quantification of the percentage of positive ECM1 staining in the liver biopsy samples from *H* with ImageJ software. In the scatter dot plot, 1 dot represents data from 1 animal or patient. The results are shown as the mean ± standard deviation. Student t test: $^{*}P < .05$, $^{***}P < .001$, $^{****}P < .0001$. SMA, smooth muscle actin.


A
AAV Injection
Percent survival
Weeks after birth
KO+AAV-NC (n=8)
KO+AAV-ECM1 (n=8)
p=0.0002
B
ECM1
Relative ECM1 mRNA Level
KO+AAV-NC
KO+AAV-ECM1
C
KO+AAV-NC
KO+AAV-ECM1
ECM1
β-actin
85KD
42KD
D
KO+AAV-NC
KO+AAV-ECM1
Masson's trichrome
SHG/TPEF
ACTA2
100μm
E
Masson's trichrome (fold change)
SHG/TPEF (fold change)
F
ACTA2
GAPDH
42KD
36KD
G
Hydroxyproline (fold change)
Expression of ACTA2/GAPDH
H
AAV injection
CCl4 injection
Sacrifice
Week
I
WT+AAV
NC
ECM1
FLAG
J
WT+AAV-NC
WT+AAV-ECM1
Sirius red
K
Sirius red (fold change)
ACTA2 (fold change)
L
M
Hydroxyproline (Fold change)

reduced liver fibrosis in ECM1-KO mice, as assessed by collagen (Masson's trichrome and SHG/TPEF) and ACTA2 staining or hydroxyproline content ($P < .0001$ by t test) (Figure 7*D*–*G*). These findings suggest that re-expressing ECM1 in hepatocytes is sufficient to ameliorate fibrogenesis in ECM1-KO mice.

We also tested the therapeutic efficacy of ectopic ECM1 expression in the chronic CCl_4 liver fibrosis mouse model. Because of the delayed AAV8-induced expression of ECM1, we injected AAV-NC and AAV-ECM1 into normal mice 1 week before the onset of CCl_4 treatment (twice a week for 6 weeks) and killed the mice 2 days after the last CCl_4 injection (Figure 7*H*). FLAG-tagged ECM1 was successfully expressed in the liver upon AAV8 infection and partially rescued the CCl_4 injury-mediated decrease in intrinsic ECM1 expression (Figure 7*I*). As a consequence, fibrosis and the number of activated HSCs were reduced in this mouse cohort ($P < .01$ by t test) (Figure 7*J*–*M*). The results strongly support the application of ECM1 as a promising drug to treat liver fibrosis in patients.

Discussion

In summary, we show, to our knowledge, a novel function of ECM1 in the liver. ECM1 inhibits latent TGFB1 activation and maintains liver homeostasis to prevent spontaneous fibrogenesis. Liver fibrosis is more severe when hepatocytes are depleted of ECM1 secretion in response to liver damage, and ECM1 supplementation can reverse fibrosis in such a setting (Supplementary Figure 9). These results support the clinical utility of ECM1 for the treatment of patients with liver fibrosis.

Extracellular matrix components directly affect cell fate, tissue organization, and function. Furthermore, the extracellular matrix is a storage site for some cytokines and growth factors.[6] Likewise, TGFB is secreted as a latent complex and deposited in the extracellular matrix at a high concentration in the healthy liver, as we have shown here. Despite this, abnormal activation of latent TGFB is prohibited, and homeostasis is maintained, but the mechanism by which this phenomenon occurs remains unknown. Here, we identified ECM1 as a critical component of the liver extracellular matrix that interferes with the activation of latent TGFB, probably via interacting with αv integrins, and thus maintains liver homeostasis. We also found that hepatocytes are the main ECM1 contributors in the liver. When hepatocytic ECM1 secretion is reduced by liver damage, TGFB is activated and released from deposited latent TGFB complexes to initiate HSC activation and fibrogenesis. Notably, re-expression of ECM1 in the liver can inhibit fibrogenesis. Thus, we have identified a new target for the treatment of liver fibrosis.

The cytokine TGFB1 plays an integral role in the regulation of fibrosis in multiple solid organs. Previous studies have shown that depletion of the αv integrin subunit from myofibroblasts inhibits fibrosis in the liver, lungs, and kidneys.[15,31] In contrast to the broader effect of αv integrin, no other solid organ developed spontaneous hepatic fibrosis in the ECM1-KO mice. TGFB activation is highly localized, and many regulators can be involved. Therefore, proteins other than ECM1 may regulate latent TGFB1 activation and fibrosis in different organs. Another important question is whether ECM1 could affect liver fibrosis in addition to inhibiting latent TGFB1 activation. Indeed, other cytokines and growth factors that can affect liver injury and fibrosis are stored in the extracellular matrix and might also be regulated by ECM1. Further studies are necessary to show the antifibrotic effects of ECM1 on other mediators and signaling pathways.

Systemic ECM1-KO mice showed spontaneous, and ultimately very severe, liver fibrosis, whereas hepatocyte-specific ECM1-KO mice did not show the same phenotype. One possible reason for this discrepancy is that hepatocytes are the major cellular source of ECM1 in the mouse liver but not the only source, and thus, some compensation by other liver cell types prohibits the strong spontaneous outcome in the liver. Nevertheless, $ECM1^{\Delta hep}$ mice were more sensitive to CCl_4 damage, suggesting a major role of this cell type in damage-mediated ECM1 down-regulation and onset of the fibrogenic response. Additionally, it is currently unclear how ECM1 affects signals in different liver cell types. Additional studies are warranted to test the effects of ECM1 depletion on other liver cell types in conditional KO mice. In summary, other liver cell types contribute to

Figure 7. Exogenous application of ECM1 rescues the mortal phenotype in ECM1-KO mice and decreases liver fibrosis in the CCl_4 model. (*A*) Survival curves of ECM1-KO mice infected with AAV-NC or AAV-ECM1 (n = 8 male mice/group). Mice were administered AAV-NC or AAV-ECM1 intravenously at 4 weeks of age. (*B*) Relative mRNA (n = 8/group) and (*C*) protein levels of ECM1 in the livers of ECM1-KO mice infected with AAV-NC or AAV-ECM1. (*D*) Histologic and IHC analyses of liver sections from ECM1-KO mice infected with AAV-NC or AAV-ECM1 stained with Masson's trichrome or an ACTA2 antibody or scanned by SHG/TPEF. Scale bar, 100 μm (SHG/TPEF) and 200 μm (Sirius Red and ACTA2). (*E*) Quantification of Masson's trichrome staining and SHG/TPEF scanning (n = 8 male mice/group). (*F*) Representative immunoblot and quantification of ACTA2 protein expression. GAPDH was used as a loading control (n = 3 male mice/group). (*G*) Hydroxyproline levels in the livers of ECM1-KO mice treated with AAV-NC or AAV-ECM1 for 4 weeks (n = 6 mice per group). (*H*) Scheme of the experimental procedure for WT mice treated with CCl_4 and injected with AAV-NC or AAV-ECM1. (*I*) Immunoblot analysis of ECM1 expression in the livers of WT mice treated with AAV-NC or AAV-ECM1. (*J*) Histologic and immunohistochemical analyses of liver sections from CCl_4-treated WT mice infected with AAV-NC or AAV-ECM1 and stained with Sirius Red and an ACTA2 antibody or scanned by SHG/TPEF. (*K*) Quantification of Sirius Red staining and SHG/TPEF scanning (n = 8 male mice/group). (*L*) Representative immunoblot and quantification of ACTA2 protein expression. GAPDH was used as a loading control (n = 3 male mice/group). (*M*) Hydroxyproline levels in the livers of CCl_4-treated WT mice infected with AAV-NC or AAV-ECM1 (n = 10 male mice/group). The results are shown as the mean ± standard deviation. Student t test: $^{*}P < .05$, $^{**}P < .01$, $^{****}P < .0001$.

ECM1 production to interfere with fibrogenesis; however, ECM1 is down-regulated solely in hepatocytes at the mRNA and protein levels upon both acute and chronic liver injury.

In patients with CLD, it is a challenge to identify those who will develop cirrhosis vs those in whom the fibrosis will reverse. Only 20% of those who chronically abuse of alcohol develop fibrosis and cirrhosis.[32] Similarly, 50% of patients with hepatitis C virus infection and 10%–20% of patients with NASH develop significant fibrosis and progress toward cirrhosis within 5–15 years.[33,34] There are many factors associated with the rapid development of fibrosis, and there are no sensitive biomarkers of individual risk for fibrosis progression.[35] Our data show significantly decreased ECM1 expression in the mouse liver during fibrosis and a negative association between the level of ECM1 expression in the liver and the speed of liver fibrogenesis. Studies are needed to determine whether level of ECM1 can be used to predict fibrosis progression in patients.

Supplementary Material

Note: To access the supplementary material accompanying this article, visit the online version of *Gastroenterology* at www.gastrojournal.org, and at https://doi.org/10.1053/j.gastro.2019.07.036.

References

1. Bataller R, Brenner DA. Liver fibrosis. J Clin Invest 2005;115:209–218.
2. Schuppan D, Afdhal NH. Liver cirrhosis. Lancet 2008;371(9615):838–851.
3. Koyama Y, Brenner DA. New therapies for hepatic fibrosis. Clin Res Hepatol Gastroenterol 2015;39(Suppl 1):S75–S79.
4. Wang P, Koyama Y, Liu X, et al. Promising therapy candidates for liver fibrosis. Front Physiol 2016;7:47.
5. Marrone G, Shah VH, Gracia-Sancho J. Sinusoidal communication in liver fibrosis and regeneration. J Hepatol 2016;65:608–617.
6. Arriazu E, Ruiz de Galarreta M, Cubero FJ, et al. Extracellular matrix and liver disease. Antioxid Redox Signal 2014;21:1078–1097.
7. Seki E, Brenner DA. Recent advancement of molecular mechanisms of liver fibrosis. J Hepatobiliary Pancreat Sci 2015;22:512–518.
8. Fabregat I, Moreno-Caceres J, Sanchez A, et al. TGF-β signalling and liver disease. FEBS J 2016;283:2219–2232.
9. Wang R, Zhu J, Dong X, et al. GARP regulates the bioavailability and activation of TGFβ. Mol Biol Cell 2012;23:1129–1139.
10. **Qin Y, Garrison BS**, Ma W, et al. A milieu molecule for TGF-β required for microglia function in the nervous system. Cell 2018;174:156–171.
11. Hinck AP, Mueller TD, Springer TA. Structural biology and evolution of the TGF-β family. Cold Spring Harb Perspect Biol 2016;8:a022103.
12. **Dong X, Zhao B**, Iacob RE, et al. Force interacts with macromolecular structure in activation of TGF-β. Nature 2017;542:55–59.
13. Shi M, Zhu J, Wang R, et al. Latent TGF-β structure and activation. Nature 2011;474:343–349.
14. Henderson NC, Arnold TD, Katamura Y, et al. Targeting of αv integrin identifies a core molecular pathway that regulates fibrosis in several organs. Nat Med 2013;19:1617–1624.
15. **Reed NI, Jo H**, Chen C, et al. The $\alpha_v\beta_1$ integrin plays a critical in vivo role in tissue fibrosis. Sci Transl Med 2015;7(288):288ra79.
16. Mathieu E, Meheus L, Raymackers J, et al. Characterization of the osteogenic stromal cell line MN7: identification of secreted MN7 proteins using two-dimensional polyacrylamide gel electrophoresis, western blotting, and microsequencing. J Bone Miner Res 1994;9:903–913.
17. Bhalerao J, Tylzanowski P, Filie JD, et al. Molecular cloning, characterization, and genetic mapping of the cDNA coding for a novel secretory protein of mouse. Demonstration of alternative splicing in skin and cartilage. J Biol Chem 1995;270:16385–16394.
18. Smits P, Poumay Y, Karperien M, et al. Differentiation-dependent alternative splicing and expression of the extracellular matrix protein 1 gene in human keratinocytes. J Invest Dermatol 2000;114:718–724.
19. Deckers MM, Smits P, Karperien M, et al. Recombinant human extracellular matrix protein 1 inhibits alkaline phosphatase activity and mineralization of mouse embryonic metatarsals in vitro. Bone 2001;28:14–20.
20. Hamada T, McLean WH, Ramsay M, et al. Lipoid proteinosis maps to 1q21 and is caused by mutations in the extracellular matrix protein 1 gene (*ECM1*). Hum Mol Genet 2002;11:833–840.
21. **Su P, Chen S, Zheng YH**, et al. Novel function of extracellular matrix protein 1 in suppressing Th17 cell development in experimental autoimmune encephalomyelitis. J Immunol 2016;197:1054–1064.
22. **Li Z, Zhang Y**, Liu Z, et al. ECM1 controls T_H2 cell egress from lymph nodes through re-expression of $S1P_1$. Nat Immunol 2011;12:178–185.
23. **He L, Gu W, Wang M**, et al. Extracellular matrix protein 1 promotes follicular helper T cell differentiation and antibody production. Proc Natl Acad Sci U S A 2018;115:8621–8626.
24. Smit JJ, Schinkel AH, Oude Elferink RP, et al. Homozygous disruption of the murine *MDR2* P-glycoprotein gene leads to a complete absence of phospholipid from bile and to liver disease. Cell 1993;75:451–462.
25. Hammad S, Cavalcanti E, Werle J, et al. Galunisertib modifies the liver fibrotic composition in the

Abcb4Ko mouse model. Arch Toxicol 2018;92:2297–2309.
26. Fondevila C, Shen XD, Moore C, et al. Cyclic RGD peptides with high affinity for $\alpha5\beta1$ integrin protect genetically fat Zucker rat livers from cold ischemia/reperfusion injury. Transplant Proc 2005;37:1679–1681.
27. George J, Roulot D, Koteliansky VE, et al. In vivo inhibition of rat stellate cell activation by soluble transforming growth factor β type II receptor: a potential new therapy for hepatic fibrosis. Proc Natl Acad Sci U S A 1999;96:12719–12724.
28. Qi Z, Atsuchi N, Ooshima A, et al. Blockade of type β transforming growth factor signaling prevents liver fibrosis and dysfunction in the rat. Proc Natl Acad Sci U S A 1999;96:2345–2349.
29. Dooley S, Hamzavi J, Breitkopf K, et al. Smad7 prevents activation of hepatic stellate cells and liver fibrosis in rats. Gastroenterology 2003;125:178–191.
30. Liu Y, Meyer C, Xu C, et al. Animal models of chronic liver diseases. Am J Physiol Gastrointest Liver Physiol 2013;304:G449–G468.
31. Henderson NC, Arnold TD, Katamura Y, et al. Targeting of α_V integrin identifies a core molecular pathway that regulates fibrosis in several organs. Nat Med 2013;19:1617–1624.
32. Schwartz JM, Reinus JF. Prevalence and natural history of alcoholic liver disease. Clin Liver Dis 2012;16:659–666.
33. Schuppan D, Schattenberg JM. Non-alcoholic steatohepatitis: pathogenesis and novel therapeutic approaches. J Gastroenterol Hepatol 2013;28(Suppl 1):68–76.
34. Kielland KB, Delaveris GJ, Rogde S, et al. Liver fibrosis progression at autopsy in injecting drug users infected by hepatitis C: a longitudinal long-term cohort study. J Hepatol 2014;60:260–266.
35. Friedman SL. Evolving challenges in hepatic fibrosis. Nat Rev Gastroenterol Hepatol 2010;7:425–436.

Author names in bold designate shared co-first authorship.

Received October 29, 2018. Accepted July 15, 2019.

Reprint requests
Address requests for reprints to: Bing Sun, PhD, MD, Shanghai Institute of Biochemistry and Cell Biology, Chinese Academy of Sciences; 320 Yue-Yang Road, Shanghai 200031, China. e-mail: bsun@sibs.ac.cn; fax: 86-21-53921326; or Jidong Jia, PhD, Liver Research Center, Beijing Friendship Hospital, Capital Medial University, 95 Yong-an Road, Xicheng District, Beijing 100050, China. e-mail: jia_jd@ccmu.edu.cn; fax: +8610-6313 9246; or Jinlin Hou, PhD, Department of Infectious Diseases, Nanfang Hospital, Southern Medical University, Guangzhou, 510515, China. e-mail: jlhousmu@163.com; fax: 86-20-616141941; or Steven Dooley, PhD, Molecular Alcohol Research in Gastroenterology, Department of Medicine II, Faculty of Medicine at Mannheim, University of Heidelberg, Germany, Theodor-Kutzer Ufer 1-3, 68167 Mannheim, Germany. e-mail: Steven.Dooley@medma.uni-heidelberg.de; fax: +49-621-383-1467.

Acknowledgments
We thank Peter ten Dijke and David A. Brenner for their discussions and comments during preparation of this manuscript.

Author contributions: Weiguo Fan, Tianhui Liu, and Wen Chen designed and conducted the experiments and data analysis. Weiguo Fan and Steven Dooley wrote the manuscript. Yadong Fu, Nan Li, Cui Liu, Yaguang Zhang, Qiaoshi Lian, Xinhao Zhao, Chenghua Yan performed research and analyzed data. Seddik Hammad and Thomas Longerich helped with IHC and immunofluorescence staining. Ingrid Hausser helped with EM analysis and performed the methylene blue staining for the revised version. Li Li, Chunyan Yi, Zhiyang Ling, and Liyan Ma performed antibody production and provided technical support. Yajing He, Xinyan Zhao, Hufeng Xu, Ping Wang, Min Cong, Hong You, Zhihong Liu, and Yan Wang performed human samples collection. Jianfeng Chen, Dangsheng Li, and Lijian Hui provided helpful suggestions, discussed data interpretation, and contributed to the manuscript. Steven Dooley, Jinlin Hou, Jidong Jia, and Bing Sun supervised the study, analyzed the data, and helped write the manuscript.

Technical assistance from Kerry Gold.

Conflicts of interest
The authors disclose no conflicts.

Funding
This work was supported by the Ministry of Science and Technology of China (2016YFA0502204), the Strategic Priority Research Program of the Chinese Academy of Sciences (XDB19000000), the National Natural Science Foundation of China (31630024) from Bing's Lab, a grant from the Ministry of Science and Technology of China (2018ZX09201016, 2018ZX10301202, 2018ZX10302204), the National Natural Science Foundation of China (81770596 and 81641022), the Wang Baoen Liver Fibrosis Foundation (CFHPC20161019), the Guangzhou Science and Technology Plan Project (201607020019), and the BMBF program LiSyM (grant PTJ-FKZ: 031 L0043).

Supplementary Materials

Generation of Ecm1$^{flox/flox}$ *Mouse Model*

Ecm1$^{flox/flox}$ mice were generated by Shanghai Model Organisms Center (Shanghai, China). This model was generated by clustered regularly-interspaced short palindromic repeats (CRISPR)/Cas9 technology in C57BL/6J mouse background. To generate the *Ecm1*-floxed line, in which exons 6–8 of the *Ecm1* allele are flanked by loxp sites, 4 independent guide RNAs (gRNAs) targeting *Ecm1* introns 5 and 8 were designed. The *Ecm1* donor vector containing flox sites flanking exons 6–8 and 2 homology arms was used as a template. The 2 gRNAs targeted to intron 5 were 5′-GAACTCAGTAACGCTGACCC-3′ and 5′-TGAGGGGTATA TAGCCTGCT-3′. The 2 gRNAs targeted to intron 8 were 5′-GCCGTCCATCCGTCCAGCTA-3′ and 5′-ACCCGACCCTCTG TACCTAC-3′. The donor vector with 4 gRNAs and Cas9 mRNA was microinjected into C57BL/6J fertilized eggs. The positive founder mice were mated to WT C57BL/6J mice to obtain *Ecm1* flox heterozygous mice. Progeny were screened by polymerase chain reaction (PCR) for germ-line transmission of the targeted alleles. The primers (P1, P2) used for genotyping were P1: 5′-AGCCCGGCCCACTTCCTTA-3′ and P2: 5′- CTTCCGATCCCTGCTTCATTTACA-3′. The PCR products were further confirmed by sequencing. *Ecm1* flox heterozygous mice were crossed with albumin-Cre mice to generate *Ecm1*$^{flox/flox}$/albumin-Cre mice.

Generation of Recombinant ECM1 Protein and Antibody

Recombinant ECM1 protein was generated in our laboratory and has been previously described.[1] The Bac-to-Bac Baculovirus Expression System (Invitrogen, Waltham, MA) was used for recombinant ECM1 production. ECM1 complementary DNA fused to the Human-Fc sequence at the C-terminus was cloned into the pFastBac vector (Invitrogen). In our subsequent experiments, we used the human IgG protein as the control group. The resulting plasmid was then used to generate recombinant baculoviruses that were then used to infect High-Five insect cells, which were grown at 27°C in suspension culture in SF-900II medium (Invitrogen). High-Five cell cultures were infected at a density of 2 ×106 cells per milliliter and used for experiments after 72 hours of infection. After 72 hours of infection at 27°C, medium containing secreted ECM1 was centrifuged (500*g* for 10 minutes) and frozen at -–80°C. Conditioned medium supplemented with protease inhibitors was then centrifuged (12,000 revolutions per minute for 60 minutes) to remove cellular debris and applied to an anti-human Fc Affinity Gel column (Orgma) equilibrated with 20 mmol/L sodium phosphate buffer, pH 7.0. The bound proteins were eluted with 0.1 mol/L glycine solution, pH 2.8. All purification steps were performed at 4°C.

Anti-mouse ECM1 primary antibodies were generated in our laboratory and have been previously described.[2] Briefly, the N- and C-terminal ECM1 rabbit polyclonal antibodies were raised against recombinant bacterially produced mouse ECM1 protein fragments encompassing N- and C-terminal peptides.

The human ECM1 antibody was made in our laboratory and is described here. Antigen for immunization and hybridoma screening: recombinant human ECM1 fused with a 6*his tag on the C-terminus (hECM1-his) was expressed by the Bac-to-Bac Baculovirus Expression System (Invitrogen) as previously described. Immunization of mice and generation of monoclonal antibodies: mouse anti-human ECM1 monoclonal antibodies were generated by Shanghai Immune Biotech (Shanghai, China). Briefly, 6-week-old female BALB/c mice were immunized subcutaneously on their backs with 100 μg of the hECM1-his tag protein in complete Freund's adjuvant. An equal amount of the hECM1-his tag protein dissolved in incomplete Freund's adjuvant was used to boost immunization on days 21 and 42. Three days before fusion, mice were intraperitoneally injected with 100 μg for the final boost. Mouse splenic cells were harvested and fused with the myeloma cell line SP2/0 using 50% polyethylene glycol (weight/volume) and plated in 96-well plates. Culture supernatants from each well were screened by enzyme-linked immunosorbent assay. Positive wells were then selected by using a limiting dilution method. After 3 cycles of cloning, positive hybridoma clones were established. The monoclonal antibody was produced from cultured hybridoma cells and purified by Protein G column chromatography.

Animal Models of Liver Fibrosis

For the CCl_4 model of liver fibrosis, adult male mice (8210 weeks old) were injected intraperitoneally with CCl_4 diluted 1:10 in corn oil (Sigma-Aldrich, St Louis, MO) or vehicle (corn oil) at 10 μL/g of body weight twice weekly for 4 or 6 weeks as indicated. Mice were killed 48 hours after the last CCl_4 injection. For the bile duct ligation model, 6-week-old male mice were anesthetized. A laparotomy was performed, the common bile duct was ligated twice, and the abdomen was closed. The sham operation was performed similarly without bile duct ligation. Mice were killed 3 and 9 days after surgery. For the NASH model, mice were fed a high-fat, methionine- and choline-deficient diet (MP Biomedicals, Santa Anna CA) ad libitum for 8 weeks. Controls were pair-fed a methionine/choline control diet (MP Biomedicals). The Institutional Animal Care and Use Committees approved all animal experiments, which were performed at the Institute Pasteur of Shanghai, Chinese Academy of Sciences.

Isolation and Culture of Mouse Primary Liver Cells

Liver cells from mice were fractionated into hepatocytes, KCs, LSECs, and HSCs. All cells were prepared from mouse livers using 2-step collagenase perfusion as described previously.[3] To remove hepatocytes, the cell suspension was centrifuged at 50*g* for 3 minutes. Then, the supernatant was centrifuged at 700*g* for 7 minutes to collect the nonparenchymal cell fraction. Nonparenchymal cells were subjected to 4-layer discontinuous density gradient

centrifugation with 7.2%, 11.2%, 13.2%, and 14.5% OptiPrep Density Gradient Medium (D1556, Sigma-Aldrich). KCs and LSEC fractions were positively selected by using fluorescence-activated cell sorting with anti-F4/80 antibody or anti-CD146 antibodies. The HSC fraction was purified by using negative selection for KCs and LSECs.

Quantitative Measurements of Collagen Content by Second-Harmonic Generation/2-Photon Excitation Fluorescence Technology

All unstained liver tissue specimens were imaged by a SHG/TPEF technology that was used to visualize collagen and cell structures (Genesis200TM, HistoIndex, Singapore). A magnified image (×20) of a specimen was captured for further image analysis. To cover most of the sample areas, 3 9-by-9 multi-tile images were acquired for each section with a final image size of 16 mm^2 (4 × 4 mm). Each image was saved at a resolution of 512 × 512 pixels. To determine only disease-related collagen, image artifacts and structural collagen in large portal tracts and blood vessels were excluded. The features of collagen fibers from portal, septal, and fibrillar areas were extracted to reflect the collagen structural information as described previously in the study of Xu et al.[4] For comparison, digitized images of liver tissue sections stained by H&E, Masson trichrome, and Sirius red were acquired using light microscopy (B X60; Olympus, Tokyo, Japan).

RNA In Situ Hybridization

We performed in situ hybridizations on fixed frozen liver tissue samples using the RNAscope system with the Fluorescent Multiplex Reagent kit V2 (catalog no. 323100; Advanced Cell Diagnostics, Newark, CA) for fluorescence development according to the manufacturer's protocols using TSA reagents (Perkin Elmer, Waltham, MA). Probes for mouse albumin (Mm-ALB-C2, 437691-C2), ECM1 (Mm-ECM1, 568221), human albumin (Hs-ALB-C2, 600941-C2), and ECM1 (Hs-ECM1, 568211) and negative and positive control probes were purchased from Advanced Cell Diagnostics. As will be described, pretreatment, hybridization, amplification, and detection were performed according to the manufacturer's protocols for fixed frozen tissue (Advanced Cell Diagnostics).

After each section was incubated with H_2O_2 for 10 minutes at room temperature, the slides were submerged in 1× Target retrieval solution for 5 minutes at ≥99°C and then sequentially washed with distilled water and 100% EtOH. After adding protease Plus III to each section, the sections were incubated for 30 minutes at 40°C and washed with distilled water. For detection, after adding probes to each section, the sections were incubated for 2 hours at 40°C and washed with Wash Buffer for 2 minutes. The fluorophores used were TSA Plus Cyanine 3 (Perkin Elmer, NEL744001KT) in C1 at a concentration of 1:1000 for ECM1 probes and TSA Plus Cyanine 5 (Perkin Elmer, NEL745001KT) in C2 or C3 at a concentration of 1:3000 for ALB probes and at a concentration of 1:750 for other probes. Sections were counterstained with 4′,6-diamidino-2-phenylindole (fluorescent) for 30 seconds to detect nuclei, and slides were coverslipped with fluorescent mounting medium.

Quantitative Real-Time Polymerase Chain Reaction

Total RNA was extracted from tissues and cells using TRIzol (Invitrogen). The purified RNA (1 μg) was quantified and reverse-transcribed using a ReverTraAce qPCR RT Kit (Toyobo, Osaka, Japan). The expression levels of the mRNA transcripts were calculated relative to the expression of GAPDH by using the formula $2^{-\Delta CT}$. Supplementary Table 1 lists the primers used in the experiments.

Immunoblotting

All organs and cells were lysed in radioimmunoprecipitation assay buffer, and protein levels were quantified using a BCA Protein Assay Kit (Thermo Fisher Scientific, Waltham, MA). In the polyacrylamide gel electrophoresis, each lane contained 20-μg of total protein. Primary antibodies specific for the following proteins were purchased from Abcam: actin (ab11003); SMAD3 (ab40854); and phospho-SMAD3 (ab52903). Anti-mice ECM1 primary antibodies were made in our laboratory and have been previously described.[2] Horseradish peroxidase–conjugated secondary antibodies were applied and then visualized by using enhanced chemiluminescence.

Electron Microscopy

After the mice were killed, small fragments (approximately 1 mm^3) of liver were fixed overnight in a solution containing 4% paraformaldehyde, 2.5% glutaraldehyde in 0.1 mol/L phosphate-buffered saline (PBS) (pH 7.4). Tissue fragments were washed for 20 minutes in 0.1 mol/L PBS 3 times and subsequently were treated with 2% osmium tetroxide in PBS for 1.5 hours. After washing for 5 minutes × 3 with PBS, specimens were dehydrated in a graded ethanol series and embedded in EPON epoxy resin (Miller-Stephenson Chemical Company, Sylmar, CA). For orientation purposes, 1-μm sections were stained with toluidine blue. Ultrathin sections (70–80 nm) were then cut with a Reichert-Jung ultramicrotome, collected on formvar-coated nickel grids, and stained with uranyl acetate for 10 minutes and with lead citrate for 7 minutes. Samples were examined with an FEI (Hillsboro, OR) Tecnai G2 Spirit transmission electron microscope.

Immunohistochemistry and Immunofluorescence Staining

Mouse and human liver sections for IHC analyses were deparaffinized, rehydrated, and incubated with anti-α–smooth muscle actin (SMA) (1:200, ab7817) and anti-human ECM1 (1:100, made in our laboratory) antibodies. Sections for immunofluorescence staining were incubated with anti-mouse ECM1 (1:200, made in our laboratory) and anti-αv integrin (1:60, sc-376156) primary antibodies

followed by Alexa Fluor 594- and Alexa Fluor 488-conjugated secondary antibodies (all from eBioscience, Waltham, MA) and then imaged via fluorescence microscopy.

To visualize resident liver macrophages (KCs), IHC of formalin-fixed, paraffin-embedded (FFPE) liver sections were used. After deparaffinization and rehydration, antigen demasking was performed in heated citrate buffer. After washing steps, slides were incubated with endogenous peroxidase blocker (Dual Endogenous Enzyme-Blocking Reagent, no. S2003; Agilent, Santa Clara, CA) for 30 minutes. After washing in 1× PBS, unspecific binding was blocked by 3% bovine serum albumin (BSA) (Calbiochem, Darmstadt, Germany; no. 12659) for 1 hour. Without washing, the slides were incubated with avidin and biotin (Endogenous Avidin/Biotin Blocking Kit, no. ab64212; Abcam, Cambridge, UK) according to manufacturer's protocol. Rat anti-F4/80 (BioRad, Hercules, CA; MCA497, 1:100) was diluted in 0.3% BSA, and the slides were incubated overnight at 4°C. After 3 washing steps in 1× PBS, biotinylated goat anti-rat IgG (Vector Laboratories, Burlingame, CA; no. BA-9400, 1:200) was diluted in 0.3% BSA, and slides were incubated for 30–45 minutes, then developed briefly with 3,3′-diaminobenzidine tetrahydrochloride (no. D5905, Sigma-Aldrich). After thorough washing, slides were counterstained with hematoxylin (Merck, Kenilworth, NJ; no. 1051742500) for 3 minutes and mounted. Images were captured by Leica (Wetzlar, Germany) DMRE microscope.

To investigate metabolic zonation, liver microvessels, bile network, and ductular reaction, co-immunofluorescence staining was done according to Hammad et al with slight modifications.[5] Briefly, formalin-fixed, paraffin-embedded liver sections were incubated overnight with primary antibodies as follows: rabbit anti-GS (Sigma-Aldrich, no. G2781; 1:2000) and goat anti-mouse dipeptidyl peptidase IV (DPPIV/CD26, no. AF954, 1:100; R&D Systems, Minneapolis, MN), or goat anti-mDPPIV/CD26 (R&D Systems, no. AF954, 1:100) and rabbit anti-intercellular adhesion molecule 1 (ICAM1, no. 10020-1-AP, 1:100; Proteintech, Rosemont, IL), or rabbit ant-dytokeratin19 (CK19, no. 14965-1-AP, 1:100; Proteintech). After washing in 1× PBS, slides were incubated for 60 minutes with secondary antibodies as follows: Alexa Fluor 488 conjugated donkey anti-goat IgG (Dianova, Hamburg, Germany; no. 705-546-147, 1:100) and/or Cy 3 conjugated anti-rabbit IgG (Dianova; no. 711-166-152, 1:200). Then slides were counterstained using DRAQ5 Fluorescent Probe Solution (Thermo Fisher Scientific; no. 62251, 1:1000). Images were captured by a confocal microscope (Leica).

For apoptosis studies, mouse livers were stained with a terminal deoxynucleotidyl transferase–mediated deoxyuridine triphosphate nick-end labeling kit (TACS TdT In Situ–Fluorescein, no. 4812-30-K R&D Systems) according to the manufacturer's procedures. As positive controls, liver sections from fasted mice treated with 1 dose of paracetamol (acetaminophen) (200 mg/kg, intraperitoneal) were used. The livers were collected for apoptosis assay 24 hours after paracetamol exposure. After counterstaining with DRAQ5 Fluorescent Probe Solution, slides were scanned using a confocal microscope (Leica).

Supplementary Table 2 lists the reagents, antibodies, and kits used in the experiments.

Transforming Growth Factor β Activation Assay

Primary HSCs from WT mice cultured in 24-well plastic culture plates were cocultured with NIH-3T3 cells, stably expressing a luciferase reporter vector containing 4 repeats of a SMAD binding element upstream of the minimal promoter of the firefly luciferase encoding region (obtained from Signosis, Santa Clara, CA; SL-0030-FP). Reporter cells were cultured without fetal bovine serum for 48 hours before coculture to avoid the effects of TGFB in serum. Cells were cultured in presence of recombinant mouse ECM1, cyclic arginine-glycine-aspartic acid peptide (BML-P700; Enzo, New York, NY), CWHM-12 (HY-18644; MedChemExpress, Monmouth Junction, NJ) or control protein (human IgG) for 16 hours, and TGF-β activity was calculated from luminescence measurements.

Quantification of Hepatic Collagen Content

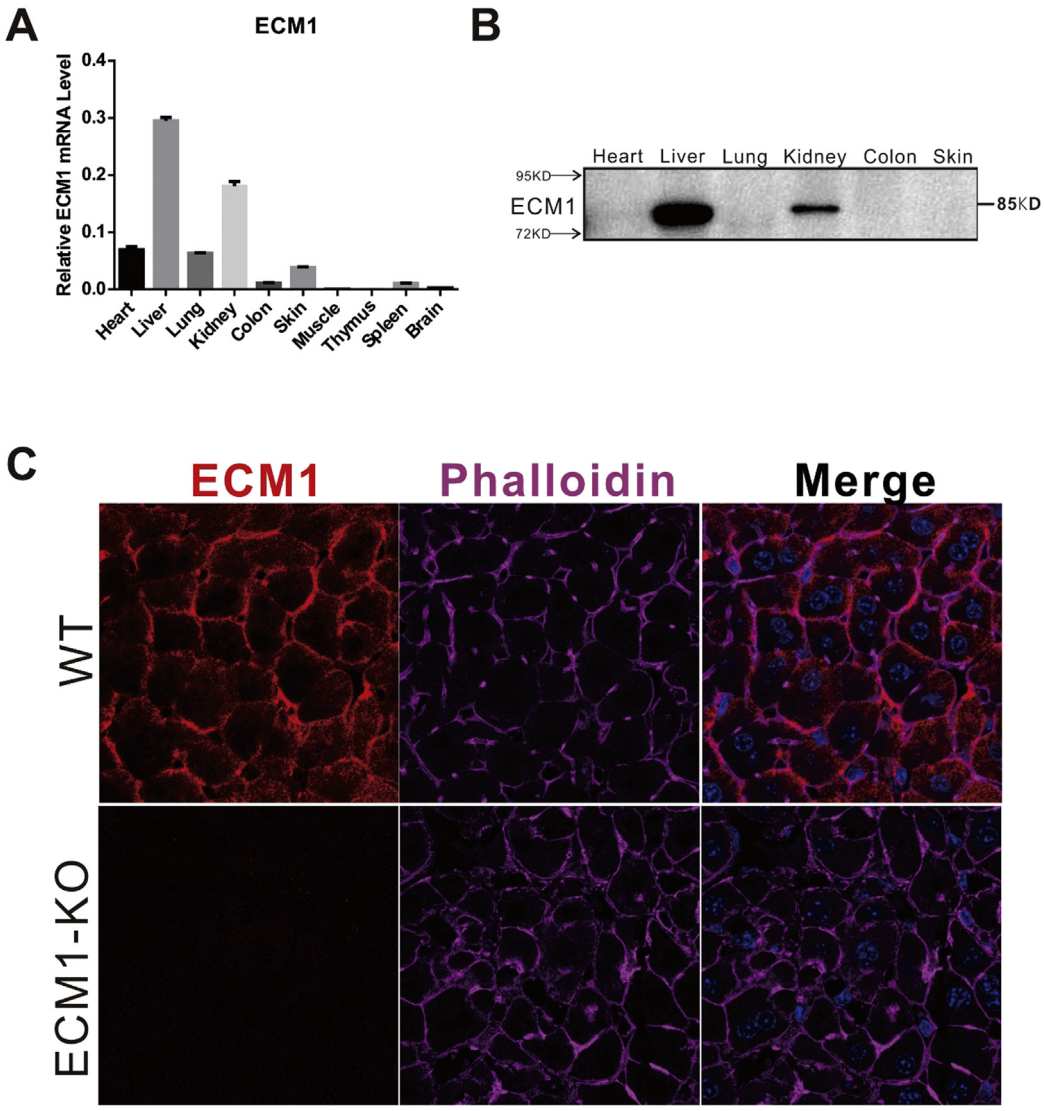
Intrahepatic collagen deposition was determined by using H&E, Masson's trichrome, and Sirius Red staining, as described previously.[6] Hydroxyproline content was quantified colorimetrically in 0.1-g liver samples with a hydroxyproline detection kit (Jiancheng Institute of Biotechnology, Nanjing, China) according to the manufacturer's instructions. Briefly, liver tissue was lysed in NaOH at 95°C for 20 minutes. The pH was adjusted to 6.0–6.8, and the lysates were incubated with reagents provided in the kit. The absorbance of the reaction products was detected at a 550-nm wavelength. Hydroxyproline concentration was calculated by using a hydroxyproline standard and normalized to the weight of the mouse liver tissue.

Adeno-associated Virus 8–Mediated Gene Expression

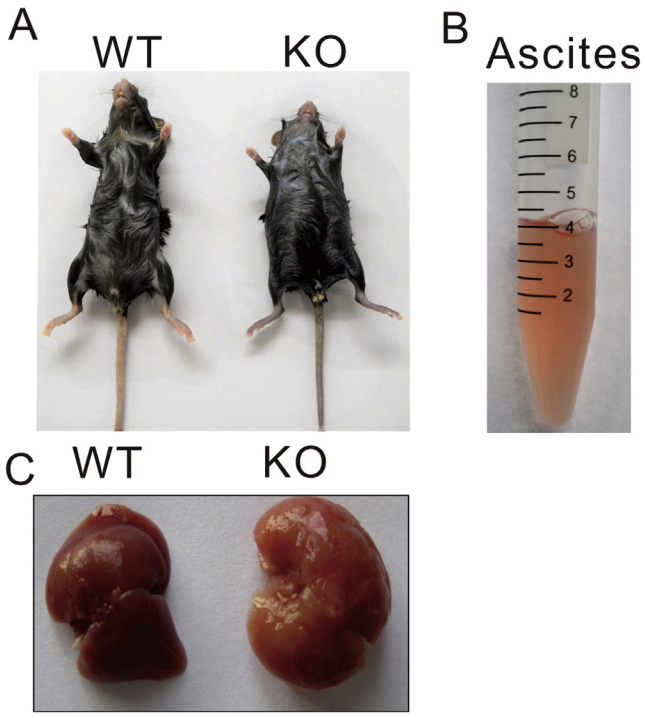
An AAV8 delivery system was used to overexpress murine soluble TGF-β type II receptor (Met1-Asp184, NM_009371.3) with a human IgG Fc tag (sTGFBR2) or ECM1 (NM_007899.3) in mouse livers. Those genes were cloned into an AAV8 package vector pAAV-T2A-GFP. Briefly, the open reading frame encoding Flag-tagged sTGFBR2 or ECM1, without a stop codon, was cloned on the 5′ end of T2A-GFP to create pAAV-sTGFBR2-T2A-GFP or pAAV-ECM1-T2A-GFP, respectively. After transcription, the T2A-sequence–encoded short peptide mediates a translational skip and yields 2 separated polypeptides, that is, GFP and either sTGFBr2 or ECM1. The pAAV-T2A-GFP (the plasmid used in the AAV8-negative control group) served as a control. AAV8 package vectors were sent to Obio Technology (Shanghai, China) for AAV8 package and purification. The mice were injected with 100 μL of virus containing 2.5×10^{11} AAV8 vector genomes via the tail vein.

Supplementary References

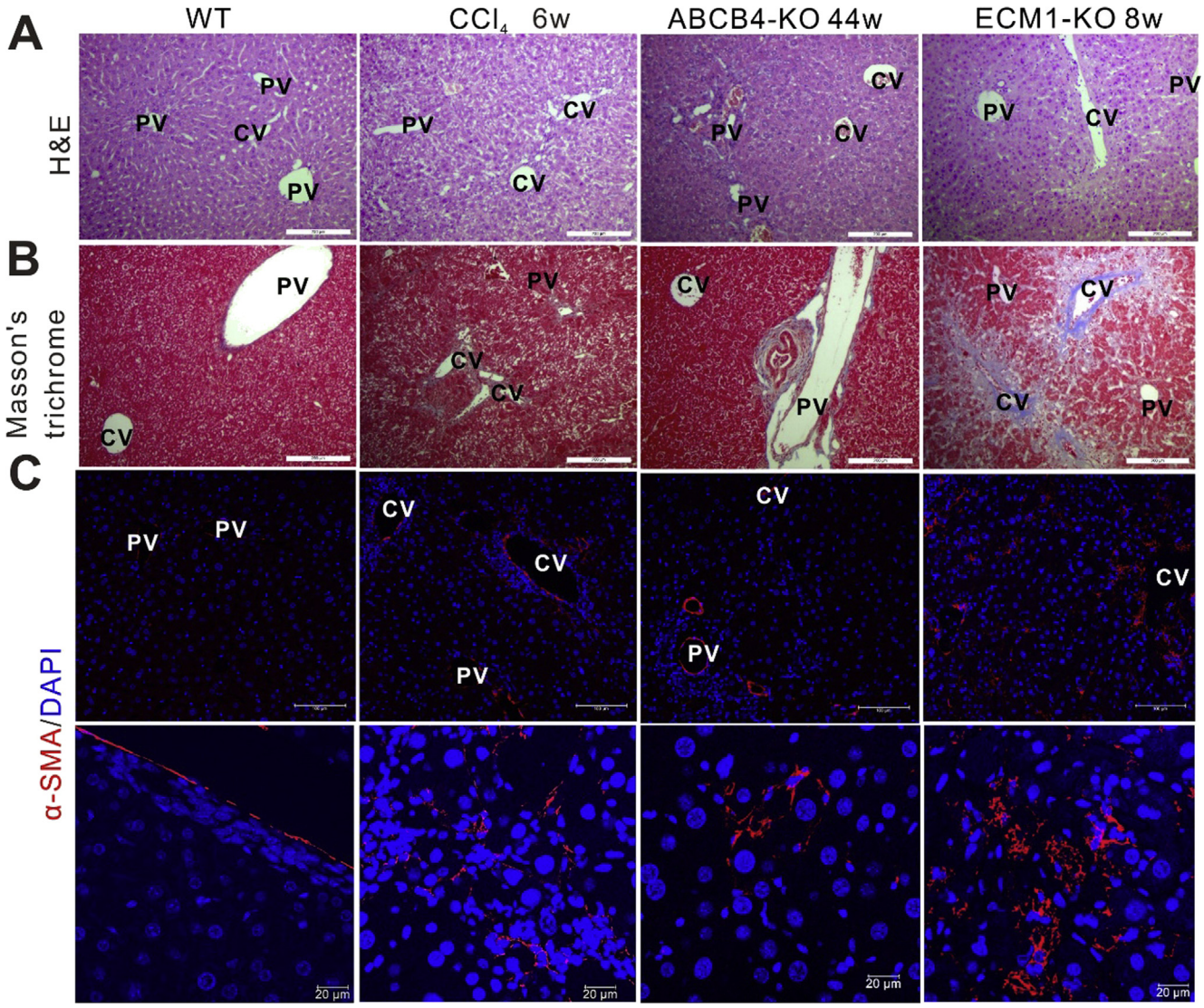
1. Su P, Chen S, Zheng YH, et al. Novel function of extracellular matrix protein 1 in suppressing Th17 cell development in experimental autoimmune encephalomyelitis. J Immunol 2016;197:1054–1064.
2. Li Z, Zhang Y, Liu Z, et al. ECM1 controls T_H2 cell egress from lymph nodes through re-expression of $S1P_1$. Nat Immunol 2011;12:178–185.
3. Chang W, Yang M, Song L, et al. Isolation and culture of hepatic stellate cells from mouse liver. Acta Biochim Biophys Sin (Shanghai) 2014;46:291–298.
4. Xu S, Wang Y, Tai DCS, et al. *q*Fibrosis: a fully-quantitative innovative method incorporating histological features to facilitate accurate fibrosis scoring in animal model and chronic hepatitis B patients. J Hepatol 2014;61:260–269.
5. Hammad S, Hoehme S, Friebel A, et al. Protocols for staining of bile canalicular and sinusoidal networks of human, mouse and pig livers, three-dimensional reconstruction and quantification of tissue microarchitecture by image processing and analysis. Arch Toxicol 2014;88:1161–1183.
6. Breitkopf-Heinlein K, Meyer C, König C, et al. BMP-9 interferes with liver regeneration and promotes liver fibrosis. Gut 2017;66:939–954.



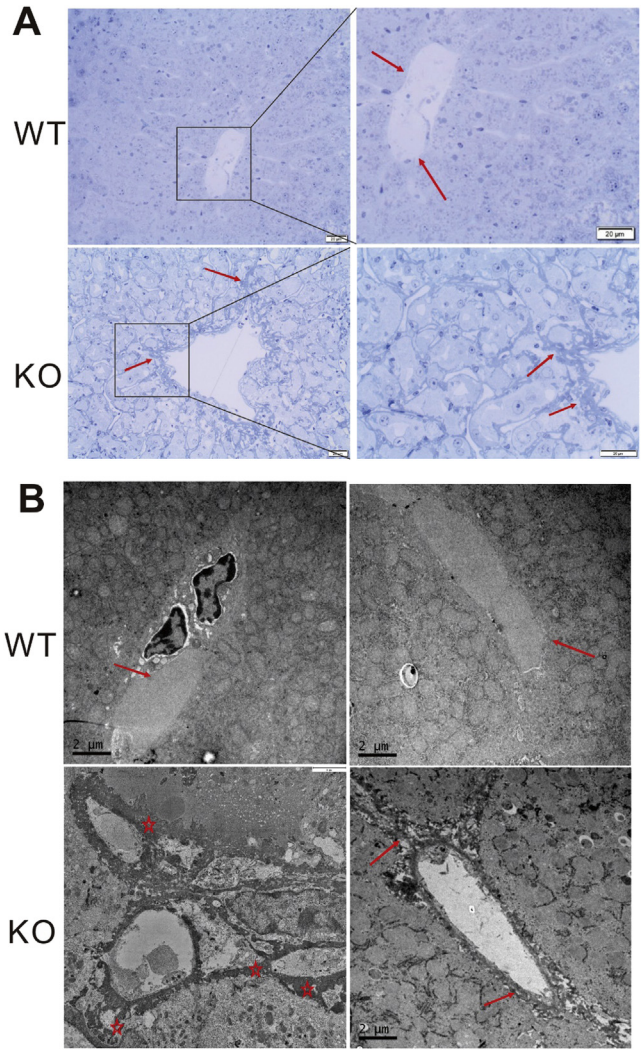
Supplementary Figure 1. ECM1 protein localizes in the extracellular matrix of normal liver. Expression of ECM1 (*A*) mRNA and (*B*) protein in different organs of healthy wild-type mice. Tissues were lysed in Trizol or radioimmunoprecipitation assay buffer. Protein levels in radioimmunoprecipitation assay buffer were quantified with a bicinchoninic acid assay (BCA) test. Each lane contains 20 μg of total protein. (*C*) Immunofluorescence staining of ECM1 in WT and KO mouse liver; phalloidin staining is used to display cell membranes.



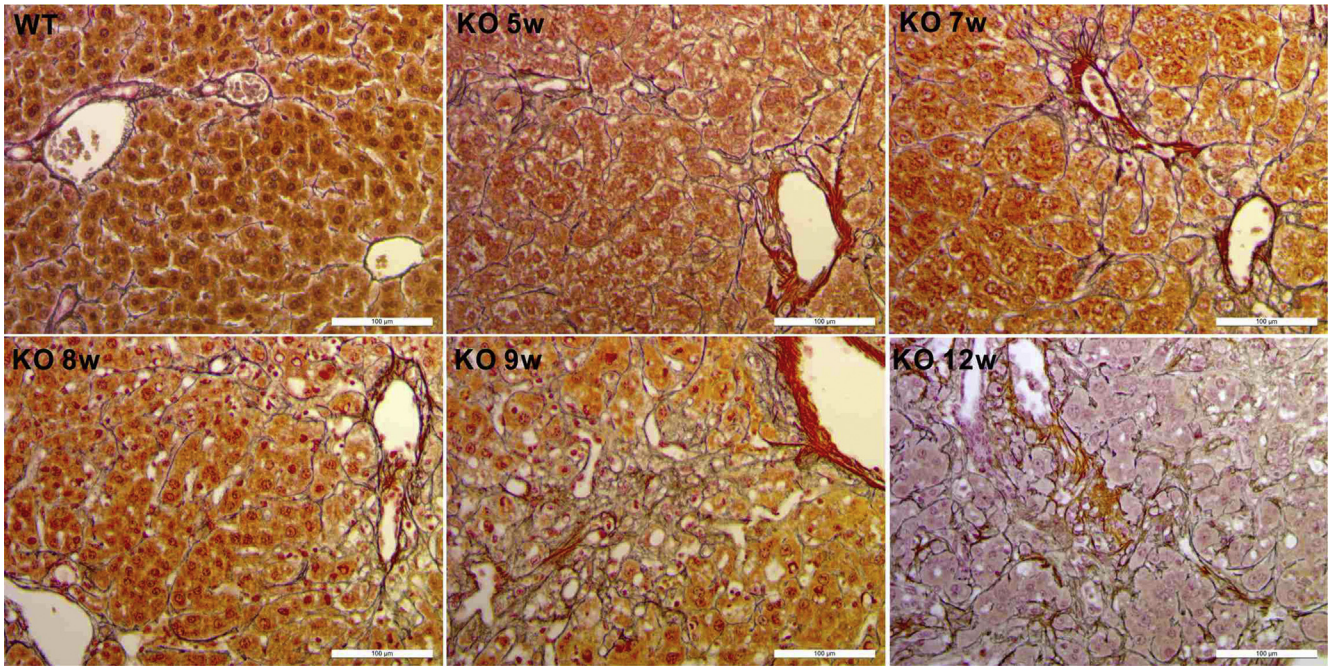
Supplementary Figure 2. ECM1-KO mice show macroscopic symptoms of severe fibrosis. (*A*) Representative picture of 8-week-old ECM1-WT and -KO mice. (*B*) Ascites, collected from a representative 8-week-old ECM1-KO mouse. (*C*) Representative photo of livers from 8-week-old ECM1-WT and -KO mice.



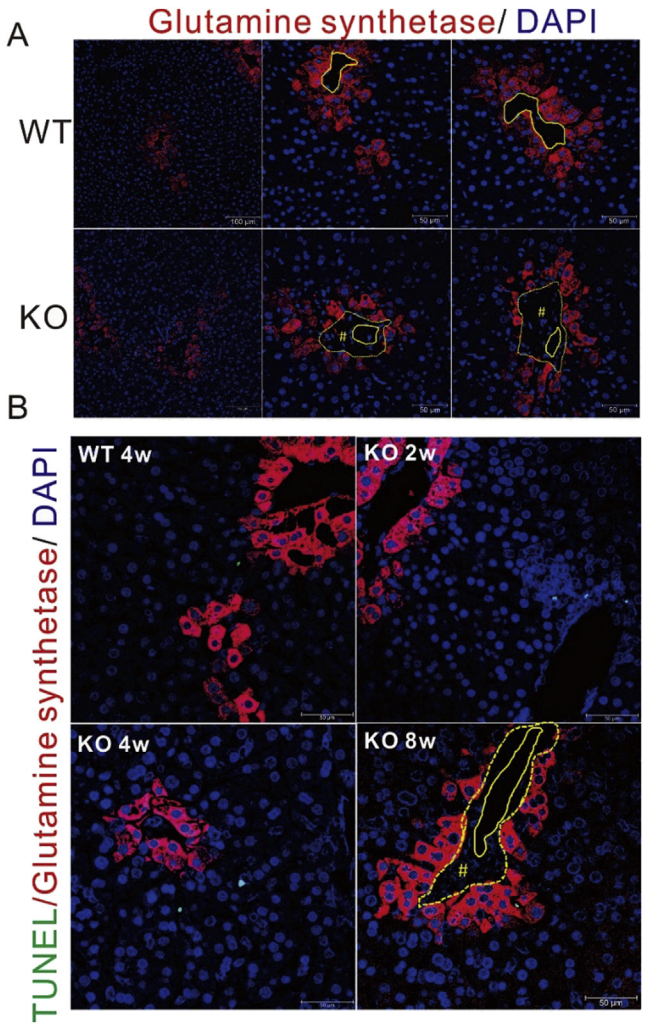
Supplementary Figure 3. ECM1-KO mice spontaneously develop symptoms of severe liver fibrosis at 8 weeks after birth. PV, portal vein; CV, central vein. Representative histologic and immunofluorescent images of liver sections from 8-week-old ECM1-WT and -KO mice: (*A*) H&E, (*B*) Masson's trichrome, and (*C*) α-smooth muscle actin, as compared to diseased livers from 6 weeks chronic CCl_4-treated and 44-week-old ABCB4-/MDR2-KO mice. ECM1-KO mice display a severely disrupted liver architecture with more collagen deposition and stellate cell activation compared with controls and the other animal models. Scale bars: (*A*, *B*) 200 μm, (*C*, *upper*) 100 μm, and (*C*, *lower*) 20 μm.



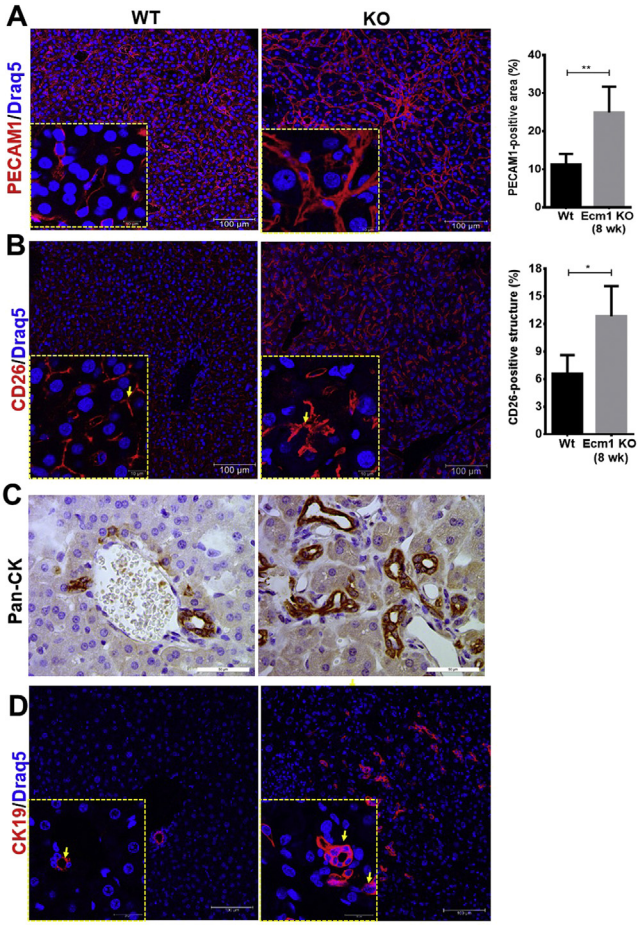
Supplementary Figure 4. ECM1-KO mice display an excessive deposition of basal membrane material and layer multiplication. (*A*) Methylene blue staining of livers from ECM1-WT and -KO mice. Scale bar, 20 μm (*B*) Transmission electron microscopy images of an ultrathin section of the liver from ECM1-WT and -KO mice. Scale bar, 2 μm. Red stars/arrows show deposition of basal membrane material/basal layer multiplication.



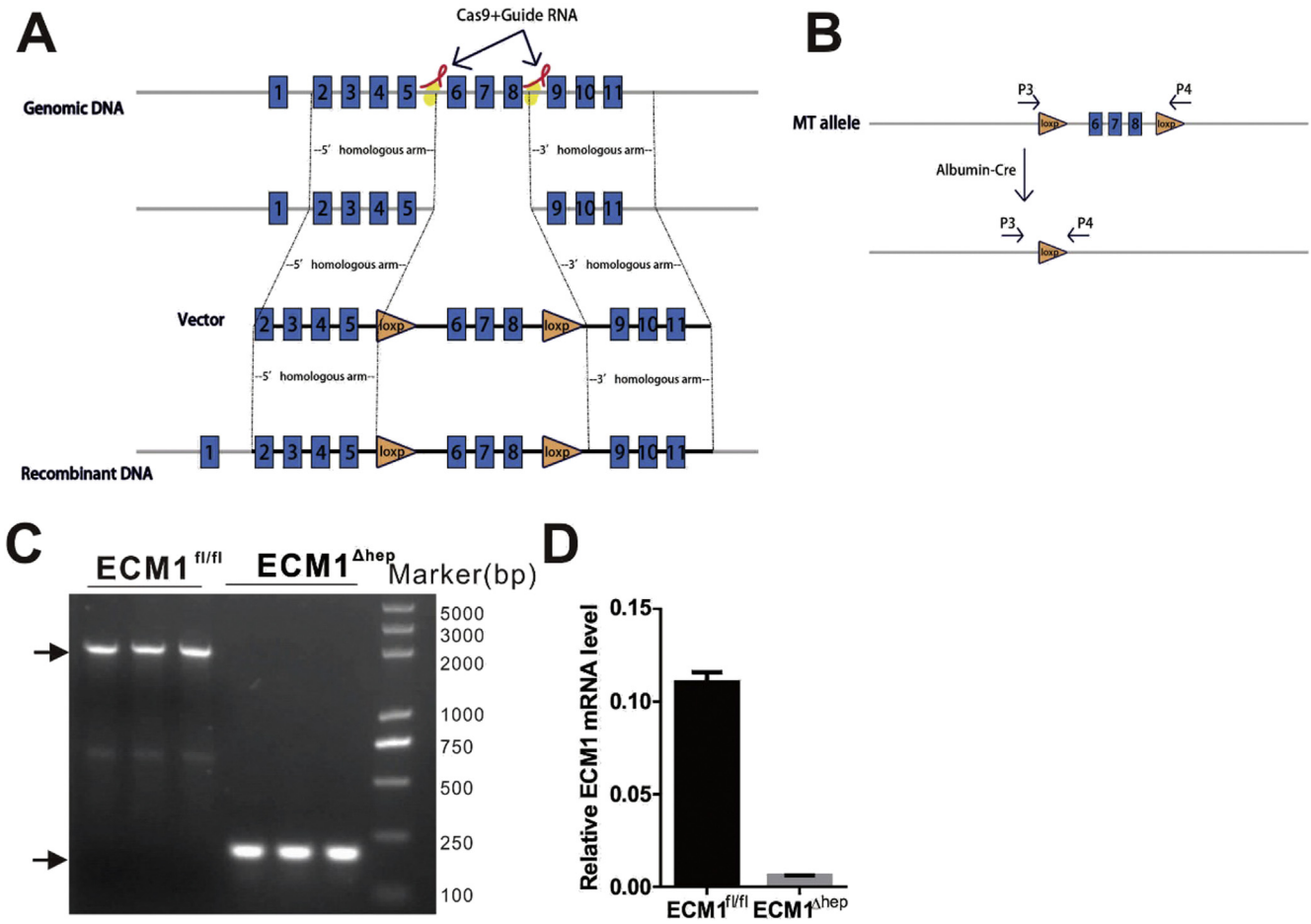
Supplementary Figure 5. Gomori stain shows reticulin and extracellular matrix deposition in ECM1-KO compared with WT mice. Representative Gomori images of WT and ECM1-KO livers from mice at different ages, as indicated. Scale bars, 100 μm.



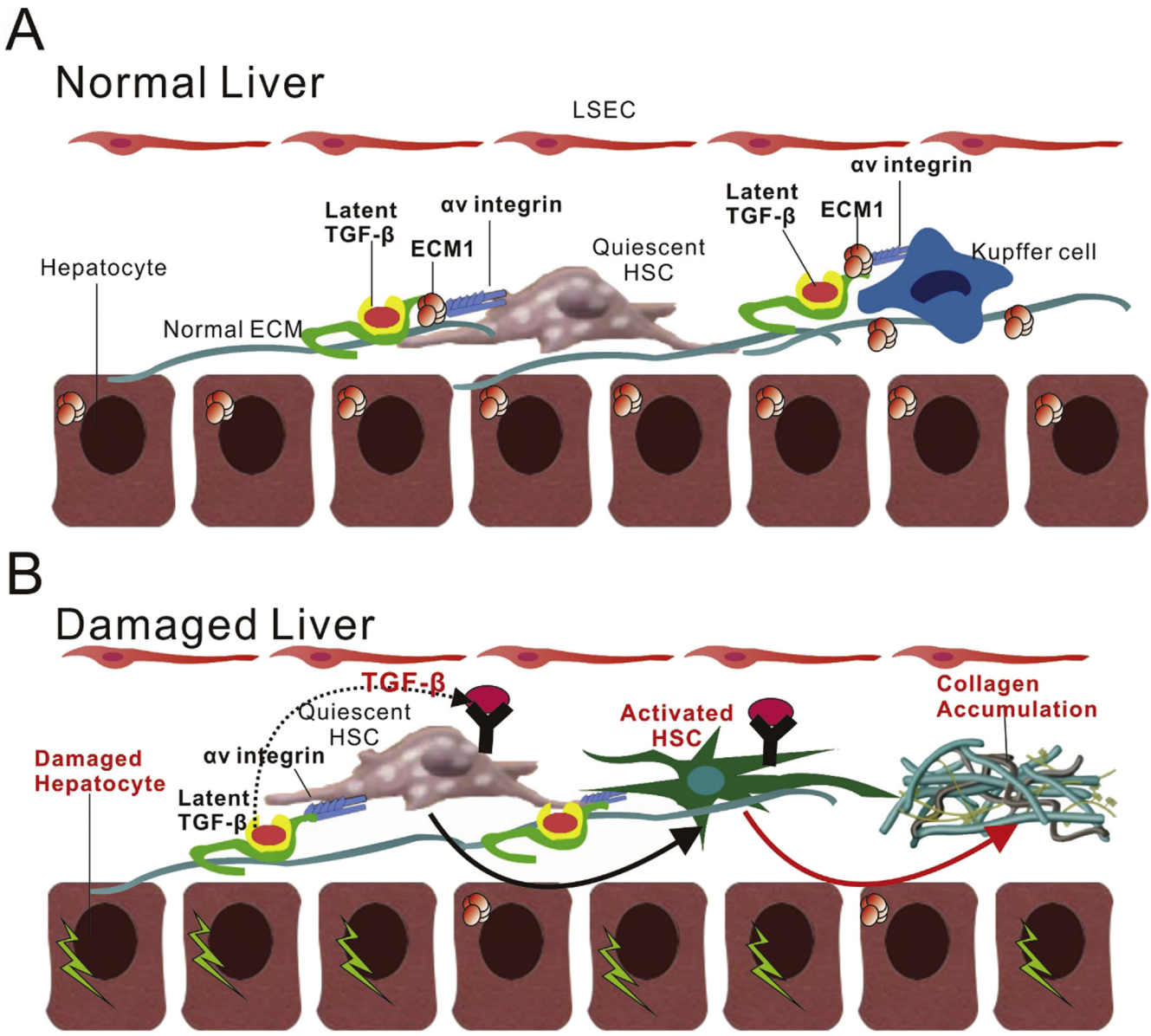
Supplementary Figure 6. ECM1-KO mice have lost the first layer of GS-expressing cells. (*A*) GS staining shows that the first layer of positive cells is lost in ECM1-KO mice compared with controls. (*B*) TUNEL staining. The continued yellow line indicates the lining of the central veins, and the dashed yellow line refers to the boundary of non-GS positive areas surrounding the central veins. The area marked with # indicates the lost GS cell layer (as compared with the controls). DAPI, 4′,6-diamidino-2-phenylindole; TUNEL, terminal deoxynucleotidyl transferase–mediated deoxyuridine triphosphate nick-end labeling.



Supplementary Figure 7. ECM1 depletion strongly disturbs the vessel systems in the liver. (*A*, *B*) Representative images and quantification of immunofluorescence analyses on liver sections from ECM1-WT and -KO mice at 8 weeks of age, stained with PECAM1(CD31) and ICAM-1/CD26 (counted from 10 different fields in each sample, 2 samples from each mouse, n = 8 male mice were examined). Sinusoidal and bile canalicular network densities are significantly increased; several bile canalicular intersection nodes are visible (*B*, *yellow arrows*) in ECM1-KO mice. (*C*, *D*) IHC and immunofluorescence analyses of liver sections from ECM1-WT and -KO mice, stained with (*C*) Pan-CK and (*D*) CK19. Pan-CK IHC and CK-19 immunofluorescence show presence of a ductular reaction (*yellow arrows*) in the portal compartment of the liver.



Supplementary Figure 8. Generation of hepatocyte-specific ECM1 conditional KO mice. (*A*, *B*) Scheme showing generation of ECM1 $^{fl/fl}$ and albumin-Cre/ECM1$^{fl/fl}$ (ECM1$^{\Delta hep}$) mice. (*C*) Genomic identification of ECM1 hepatocytes of ECM1$^{fl/fl}$ and ECM1$^{\Delta hep}$ mice. (*D*) Relative mRNA levels of ECM1 in hepatocytes from ECM1$^{fl/fl}$ and ECM1$^{\Delta hep}$ mice. bp, base pairs p, primers; MT, mutant.



Supplementary Figure 9. ECM1 is a gatekeeper in the liver that restrains TGF-β activation to maintain homeostasis and prevent fibrogenesis. (*A*) Scheme showing the mechanism of ECM1-mediated preservation of extracellular matrix (ECM)–stored latent TGF-β in normal liver. (*B*) Scheme showing a cascade of events, where ECM1 is down-regulated in hepatocytes upon liver damage to activate TGF-β in the matrix for myofibroblast generation and fibrogenesis initiation.

Supplementary Table 1. Real-Time PCR Primers

Gene	Forward 5′–3′	Reverse 5′–3′
Human ECM1	GCCAGCTCTGTGGAAGTGGA	CCGGAATCTGTTTATGCTTGC
Mouse ECM1	TGAACCAAATCTGCCTTCCTAAC	GCTGGACTGTGGTAGGTTCCA
α-SMA	GTCCCAGACATCAGGGAGTAA	TCGGATACTTCAGCGTCAGGA
Col1a1	GCTCCTCTTAGGGGCCACT	CCACGTCTCACCATTGGGG
Col3a1	AACCTGGTTTCTTCTCACCCTTC	ACTCATAGGACTGACCAAGGTGG
Desmin	GTGGATGCAGCCACTCTAGC	TTAGCCGCGATGGTCTCATAC
TGF-β1	CTCCCGTGGCTTCTAGTGC	GCCTTAGTTTGGACAGGATCTG
GAPDH	AGGTCGGTGTGAACGGATTTG	TGTAGACCATGTAGTTGAGGTCA

Supplementary Table 2. Reagents, Antibodies, and Kits Used in IHC and IF Staining

Application	Reagent/antibody/kit	Company/catalog number	Host	Dilution	Antigen retrieval	Notes
IHC	α-SMA	Dako M0851	Mouse	1:500	Citrate buffer, pH 6.0	—
IF	GS	Sigma-Aldrich G2781-100UL	Rabbit	1:1000	Citrate buffer, pH 6.0	—
IHC	Pan-cytokeratin	Dako Z0622	Rabbit	1:500	Citrate buffer, pH 6.0	—
IF	CK19	Proteintech 14965-1-AP	Rabbit	1:50	Citrate buffer, pH 6.0	—
IF	I-CAM	Proteintech 10020-1-AP	Rabbit	1:50	Citrate buffer, pH 6.0	—
IHC	Collagen IV	Dako M0785	Mouse	1:100	Citrate buffer, pH 6.0	—
IHC	Laminin	Abcam ab210959	Mouse	1:100	Citrate buffer, pH 6.0	—
IF	CD26/DPPIV	R&D Systems	Goat	1:50	Citrate buffer, pH 6.0	—
IF	CD31 (PECAM-1)	Cell Signaling Technology no.3528S	Rabbit	1:100	Citrate buffer, pH 6.0	—
IF	Anti-rabbit Cy3	Jackson ImmunoResearch 711-166-152	Donkey	1:200		—
IF	Anti-goat Cy3	Jackson ImmnoResearch 705-165-147	Donkey	1:200		—
IHC	Anti-mouse conjugated HRP	Dako P0447	Goat	1:200		—
IHC	Anti-rabbit conjugated HRP	Dako P0217	Swine	1:200		—
	Periodic acid–Schiff stain kit	Abcam ab150680				No tissue digestion with diastase
	In Situ Cell Death Detection Kit, Fluorescein	Sigma Aldrich 11684795910				—

HRP, horseradish peroxidase; IF, immunofluorescence.